1 **Insights into Early Earth from the Pt-Re-Os isotope and Highly**

2 **Siderophile Element abundance systematics of Barberton komatiites**

3

4

5

6

7 Igor S. Puchtel[1], Richard J. Walker[1], Mathieu Touboul[1],

8 Euan G. Nisbet[2], and Gary R. Byerly[3]

9

10 [1]Department of Geology, University of Maryland, 237 Regents Drive, College Park, MD 20742, USA
11 [2]Department of Earth Sciences, Royal Holloway, University of London, Egham TW20 0EX, UK
12 [3]Department of Geology and Geophysics, Louisiana State University, Baton Rouge, LA 70803, USA

13

14

15

16

17 Corresponding author:

18 Igor S. Puchtel

19 e-mail: ipuchtel@umd.edu

20
21
22
23
24

28

29   **Abstract**

30   Platinum-Re-Os isotopic and highly siderophile element (HSE: Os, Ir, Ru, Pt, Pd, and Re)

31   abundance data are reported for well-preserved komatiites from the Komati and Weltevreden

32   Formations of the Barberton Greenstone Belt, South Africa. The Re-Os data for whole-rock

33   samples and olivine and chromite separates define isochrons with ages of 3484±38 and 3263±12

34   Ma for the Komati and Weltevreden systems, respectively. The respective initial $^{187}Os/^{188}Os =$

35   0.10335±15 ($\gamma^{187}Os$ = +0.34±0.15) and 0.10442±4 ($\gamma^{187}Os$ = -0.14±0.04) are within the

36   chondritic range. When considered together with the Re-Os data for late Archean komatiite

37   systems, these data indicate that the mantle sources of most Archean komatiites evolved with

38   essentially chondritic long-term Re/Os. By contrast, the initial $^{186}Os/^{188}Os$ = 0.1198283±9

39   ($\varepsilon^{186}Os$ = -0.12±0.08) and 0.1198330±8 ($\varepsilon^{186}Os$ = +0.22±0.07) for the Komati and Weltevreden

40   systems, respectively, are non-chondritic, indicating that the mantle sources of these two

41   komatiite systems evolved with fractionated time-integrated Pt/Os. These new $^{186,187}Os$ isotopic

42   data for the early Archean komatiite systems, combined with published $^{142,143}Nd$ and ^{176}Hf

43   isotopic data for the same rocks, are consistent with formation and long-term isolation of deep-

44   seated mantle domains with fractionated time-integrated Sm/Nd, Lu/Hf, and Pt/Os ratios, at ca.

45   4400 Ma. These domains may have been generated as a result of late-stage crystallization of a

46   primordial magma ocean involving Mg-perovskite, Ca-perovskite and Fe-Pt alloys acting as the

47   fractionating phases. The inferred mantle domains were sampled by the early Archean

48   komatiites, but were largely mixed away by 2.7 Ga, as evidenced by uniform, time-integrated

49   Sm/Nd, Lu/Hf, and Pt/Os ratios inferred for the sources of most late Archean komatiite systems.

50   The total Pt and Pd abundances present in the sources of the early Archean komatiite systems are

51   calculated to be between 60-70% of those present in the estimates for the modern primitive

52   mantle. These are within the range of the total Pt and Pd abundances present in the sources of

53   late Archean komatiite systems, indicating little change in the HSE abundances in the Archean

54   mantle between 3.5 and 2.7 Ga. The new HSE data for the early Archean komatiite systems may

55   implicate late accretion of HSE to the mantle prior to completion of crystallization of a final

56   terrestrial magma ocean, followed by sluggish mixing of diverse post-magma ocean domains,

57   characterized by variably fractionated lithophile element and HSE abundances.

58

59

62

63

1. Introduction

Precisely determining the absolute and relative abundances of the highly siderophile elements (HSE; including Re, Os, Ir, Ru, Pt, and Pd) in the early terrestrial mantle is crucial for understanding such fundamental planetary processes as the Earth's primary separation of metallic core from silicate mantle (Righter, 2003), continued accretion following core formation (Morgan et al., 1981; Morgan, 1985, 1986; Walker, 2009), differentiation of the mantle (Walker et al., 1989), recycling of oceanic lithosphere (Walker et al., 1991; Hauri and Hart, 1993; Lassiter and Hauri, 1998), mass transfer in subduction zones (Brandon et al., 1996; Alves et al., 1999; Brandon et al., 1999; Woodland et al., 2002; Penniston-Dorland et al., 2012), and, possibly, inner core crystallization and core-mantle exchange (Walker et al., 1995; Brandon et al., 1998; Puchtel and Humayun, 2000; Puchtel et al., 2005).

The absolute HSE abundances and initial ^{186,187}Os/^{188}Os, that reflect the time-integrated Pt/Os and Re/Os in mantle domains, have previously mainly been estimated for relatively recent upper mantle via studies of ophiolites, abyssal peridotites, orogenic lherzolites, and mantle xenoliths representing subcontinental lithospheric mantle (Morgan et al., 1981; Morgan, 1986; Snow and Reisberg, 1995; Rehkämper et al., 1997; Handler and Bennett, 1999; Brandon et al., 2000; Meisel et al., 2001; Walker et al., 2002; Luguet et al., 2003; Pearson et al., 2004; Becker et al., 2006; Luguet et al., 2007; Liu et al., 2009; Fischer-Gödde et al., 2011). Most Re-Os isotopic data for young mantle materials and mantle-derived lavas suggest that the convecting upper mantle,

83   on average, has evolved with Re/Os broadly within the range of chondritic meteorites (Walker,

84   2009). The more limited Pt-Os isotopic data are likewise consistent with the average mantle

85   bearing a long-term Pt/Os within the range of chondritic meteorites (Walker et al., 1997;

86   Brandon et al., 2000; Brandon et al., 2005b). Finally, the relative abundances of other HSE in

87   primitive mantle (PM) estimates have been shown to be either within or slightly outside the

88   range defined by chondritic meteorites (Becker et al., 2006; Fischer-Gödde et al., 2011).

89   Most mantle materials that have been studied for HSE and Os isotopic compositions,

90   however, have been heavily processed via melt extraction, crystal-liquid fractionation events and

91   fluid- or melt-rock interactions, the effects of which have often made it problematic to constrain

92   the HSE abundances in their respective mantle domains (e.g., Rehkämper et al., 1999a;

93   Rehkämper et al., 1999b; Becker et al., 2006; Lorand et al., 2009). In addition, these young

94   materials do not provide direct information about the HSE systematics of the Archean mantle,

95   which is the key to understanding the early stages of the Earth's evolution. The study of

96   komatiites can potentially circumvent some of these issues. Most komatiites likely formed via

97   high degrees of partial melting of mantle materials on ascent (e.g., Arndt, 1977; Arndt et al.,

98   2008), leading to the extraction of large proportions of the HSE from their mantle sources

99   (Barnes et al., 1985; Keays, 1995; Rehkämper et al., 1999b). High degree mantle melting

100   provides a mechanism for obtaining representative samples of large mantle domains that is not

101   possible with small, individual mantle samples, or lower degree melts. Because komatiitic

102   magmas are superheated, have low viscosities, and ascend rapidly (Huppert and Sparks, 1985),

103   they undergo little to no differentiation prior to emplacement. The relatively high abundances of

104   HSE in komatiitic liquids also make their HSE less prone to modification by crustal

105   contamination. Further, Archean komatiites provide information about the abundances of HSE in

106   the mantle at a time when it, undoubtedly, was less modified by processes of melt extraction and

107   re-fertilization, compared to the modern mantle. Finally, differentiation of komatiite lavas

108   usually leads to fractionation of Os from Pt and Re. The resulting range in Re/Os and Pt/Os

109   ratios among different portions of lava flows permits generation of isochrons, which can be used

110   to obtain precise geochronological information, assess closed-system behavior of the HSE, and

111   precisely determine initial Os isotopic compositions and time-integrated Re/Os and Pt/Os in the

112   sources of the lavas. Typical correlations between MgO and HSE, combined with Os isotopic

113   data, can also be used to precisely calculate absolute HSE abundances in the sources of komatiite

114   lavas (Puchtel et al., 2004b; Puchtel and Humayun, 2005; Puchtel et al., 2007; Puchtel et al.,

115   2009a; Puchtel et al., 2009b).

116   Some 25 years ago, the first terrestrial Re-Os isochron, on the 2.7 Ga Pyke Hill komatiites

117   (Walker et al., 1988), and the first HSE abundance data, on the 2.7 Ga Abitibi and 89 Ma

118   Gorgona komatiites (Crocket and MacRae, 1986; Brügmann et al., 1987), were published. Since

119   then, following major advances in analytical techniques, a large body of Os isotopic and HSE

120   abundance data on Archean and post-Archean komatiite systems has accumulated (e.g., Barnes

121   et al., 1985; Walker et al., 1991; Shirey et al., 1994; Foster et al., 1996; Shirey, 1997; Walker et

122   al., 1997; Rehkämper et al., 1999b; Walker et al., 1999; Walker and Stone, 2001; Bennett et al.,

123   2002; Gangopadhyay and Walker, 2003; Maier et al., 2003; Wilson et al., 2003; Hanski et al.,

124   2004; Gangopadhyay et al., 2005; Gangopadhyay et al., 2006; Maier et al., 2009; Fiorentini et

125   al., 2011). However, despite these very substantial advances, the number of studies of Archean

126   komatiitic systems that include complete sets of complementary HSE abundance and Pt-Re-Os

127   isotopic data, as well as lithophile trace element and isotopic data, on pristine mantle lavas,

128   remains limited. This database currently includes only a handful of late Archean localities, such

129   as the 2.9 Ga Sumozero-Kenozero (Puchtel et al., 2007), 2.8 Ga Kostomuksha (Puchtel et al.,

130   1998; Puchtel et al., 2005; Puchtel and Humayun, 2005), the 2.7 Ga Abitibi and Belingwe

131   (Puchtel et al., 2004a; Puchtel et al., 2004b; Puchtel et al., 2009b) and the 2.4 Ga Vetreny Belt

132   (Puchtel et al., 2001b; Puchtel and Humayun, 2001) komatiite systems. The early Archean record

133   is incomplete at best, with only two komatiite systems, the 3.55 Ga Schapenburg Greenstone

134   Remnant (Puchtel et al., 2009a) and the 3.26 Ga Weltevreden Formation (Connolly et al., 2011),

135   both of the Barberton Greenstone Belt (BGB) in South Africa, studied to date. This is due in part

136   to the poor state of preservation of the early Archean geological record in general, and the

137   komatiite record in particular, and in part to the extreme analytical challenges that this type of

138   study poses.

139   Komatiites of the BGB, which represents the type locality of the class of rock (Viljoen and

140   Viljoen, 1969), provide a particularly valuable source of information about the HSE systematics

141   of the early Archean mantle. First, these are the oldest recognizable komatiites on Earth, some of

142   which are also characterized by a good state of preservation of their original, magmatic features.

143   Second, these komatiites have unusual chemical compositions, including extremely high MgO

144   contents of the emplaced lavas and variable depletions/enrichments in Al and heavy rare earth

145   elements (REE). These chemical features clearly distinguish them from younger komatiites and

146   imply very specific conditions for their magma generation that apparently ceased to exist by the

147   late Archean. Third, the BGB contains a *ca.* 300 Ma record of evolution of komatiite

148   magmatism; this provides a unique opportunity to track secular changes in the absolute and

149   relative HSE abundances in the Archean mantle.

150   Here, we report HSE abundance and Re-Os and Pt-Os isotopic data for well-preserved

151   komatiites from the 3.48 Ga Komati Formation (Fm.) of the Barberton Greenstone Belt (BGB) in

152 South Africa. We also report Pt-Os isotopic data, as well as additional HSE abundance and Re-

153 Os isotopic data to those reported by Connolly et al. (2011), for the 3.26 Ga Weltevreden Fm. of

154 the BGB. These early Archean komatiite systems, together with the 3.55 Ga Schapenburg system

155 studied by Puchtel et al. (2009a), are particularly interesting with respect to early Earth evolution

156 in that they formed at a time when it has been speculated that HSE abundances in the komatiites

157 were increasing due to the simple downward mixing of a veneer of HSE-rich materials added to

158 Earth by late accretion (Maier et al., 2009; Fiorentini et al., 2010).

159   New data reported here are used to reconstruct the absolute and relative HSE abundances in

160 the early Archean mantle, and to discuss implications for early terrestrial accretion history in

161 view of these data, combined with the lithophile trace element and isotope systematics for these

162 (Puchtel et al., 2013), as well as the HSE systematics for the well-studied late Archean komatiite

163 systems.

164

165 **2. Geological background and sampling**

166   The BGB is located in the Kaapvaal Craton, one of the best preserved areas of pristine

167 Archean crust on Earth, and consists of a succession of supracrustal rocks, ranging in age from

168 3.55 to 3.22 Ga, that make up three main lithostratigraphic units of ~15 km in total thickness: the

169 lower, mostly volcanic, Onverwacht Group, and the upper, predominantly sedimentary, Fig Tree

170 and Moodies Groups (Lowe, 1994, 1999; Lowe and Byerly, 1999, 2007). The Onverwacht

171 Group includes several formations; komatiites from the Komati and Weltevreden Fms. are the

172 subject of this study. The age of the Komati Fm. was determined to be 3482 ± 5 Ma using the U-

173 Pb zircon method on a thin layer of dacitic tuff (Armstrong et al., 1990). The emplacement age

174   of the komatiitic lavas from the Weltevreden Fm. was recently directly determined to be 3266±8

175   Ma using the Re-Os geochronometer (Connolly et al., 2011).

176   The Komati Fm. is divided into lower (1.8 km thick) and upper (1.3 km thick) members, with

177   komatiites dominating the Lower Komati, and komatiitic basalts being prevalent in the Upper

178   Komati (Viljoen et al., 1983; Dann, 2000). Abundances of some HSE in the Komati Fm.

179   komatiites were previously reported by Maier et al. (2003). The absolute HSE abundances were

180   found to be relatively low, which was attributed by these authors to the retention of the HSE in

181   sulfides in the mantle source region. The HSE abundances were also found to plot with

182   significant scatter on HSE vs. MgO variation diagrams, which was interpreted by Maier et al.

183   (2003) to indicate HSE mobility during seafloor alteration and metamorphism.

184   Hand specimens for this study were collected from the Lower Komati Fm., in the type area,

185   at the hillcrest of the locality illustrated by Viljoen et al. (1983) in their Fig. 3, and by Viljoen

186   and Viljoen (1969), also in their Fig. 3. At this well-exposed and locally near-continuous 120 m

187   section, a sequence of differentiated komatiite lava flows, ranging in thickness from <1 m to >10

188   m, was identified. Fifteen whole-rock samples (plus multiple replicates) and olivine and chromite

189   separates were analyzed for HSE abundances and Pt-Os and Re-Os isotopic systematics. For the

190   whole-rock samples, we utilized the same sample powder aliquots studied by Puchtel et al.

191   (2013) for lithophile trace element and isotope systematics (see Fig. 1 in Puchtel et al. (2013) for

192   sample locations).

193   The Weltevreden Fm. is located in the northern facies of the BGB. It accumulated as a thick

194   sequence of komatiitic and basaltic volcanic rocks, komatiitic tuffs, and ultramafic intrusions

195   (Lowe and Byerly, 1999). The exact thickness of the Weltevreden Fm. is unknown, but at least a

196   few thousand meters of section are present, with individual flow units being 10 to 500 m thick

197 (Lowe and Byerly, 1999). The initial Re-Os isotopic and HSE abundance data for the

198 Weltevreden Fm. komatiites were reported by Connolly et al. (2011).

199   For this study, we again used the sample powder aliquots utilized in the Puchtel et al. (2013)

200 study. These samples were collected from three differentiated komatiite lava flows, SA501,

201 KBA12, and SA564, which are ~65 m-, 25 m-, and 23 m thick, respectively (see Fig. 2 in

202 Puchtel et al. (2013) for sample locations). Although all lava flows generally exhibit a classic

203 layered structure similar to that in the lava flows from the Komati Fm. type locality, the spinifex

204 zones are very thin, with the bulk of the lava flows consisting of cumulate komatiite. The details

205 of the field petrology and petrography have been reported in Kareem (2005), Connolly et al.

206 (2011) and Stiegler et al. (2012).

207

208 **3. Analytical techniques**

209   *3.1. Sample preparation and mineral separation*

210   The procedures for sample preparation closely followed those described in detail by Puchtel et al. (2009a) and

211 Puchtel et al. (2009b). Hand specimens of 0.5-2 kg were collected from surface outcrops and cut into 1-2 cm thick

212 slabs using a diamond saw to remove any signs of alteration. Small pieces were cut off the slabs and used to prepare

213 polished thin sections at the Institute of Geology of Ore Deposits (IGEM) in Moscow. The remaining parts of the

214 slabs were polished on all sides using SiC sandpaper to remove saw marks, washed in de-ionized water, dried, and

215 crushed in an alumina-faced jaw crusher. A 200-g aliquot of crushed sample was pre-ground in an alumina shatter

216 box, then ground to a fine powder in an alumina-faced disk mill and used for the geochemical studies. The

217 remaining crushes of the largest available and freshest samples, including BV03 and BV10 (Komati Fm.) and 501-1,

218 501-8, and 12-6 (Weltevreden Fm.) were used for mineral separation. Pure olivine and chromite separates were

219 obtained at the Institute of Geology in Petrozavodsk using the combination of heavy liquid and magnetic separation

220 techniques and handpicking.

221

222   *3.2. Highly siderophile elements*

223   *3.2.1 Re-Os isotopic and HSE abundance data.* To obtain the Re-Os isotopic and HSE abundance data, 1.3-1.6

224 g of whole-rock sample powder, 0.4-0.6 g of pure olivine, or 0.08-0.09 g of pure chromite separate, 5 mL of double-

225 purged, triple-distilled conc. HNO_3, 4 mL of triple-distilled conc. HCl, and appropriate amounts of mixed ^{185}Re-

226 ^{190}Os and HSE (^{99}Ru,^{105}Pd,^{191}Ir,^{194}Pt) spikes were sealed in double, internally-cleaned, chilled 25 mL Pyrex™

227 borosilicate Carius Tubes (CTs) and heated to 270°C for 96 h. Osmium was extracted from the acid solution by CCl$_4$

228 solvent extraction (Cohen and Waters, 1996), then back-extracted into HBr, followed by purification via

229 microdistillation (Birck et al., 1997). Ruthenium, Pd, Re, Ir, and Pt were separated and purified using anion

230 exchange chromatography (Rehkämper and Halliday, 1997). Average total analytical blanks during the analytical

231 campaign were (in pg): Re 0.29±0.06, Os 0.21±0.06, Ir 0.38±0.17, Ru 1.5±0.8, Pt 14±9, and Pd 7±2 (±2σ$_{mean}$, N =

232 9). For the whole-rock samples, the total analytical blanks for all HSE constitute less than 0.7% of the total element

233 analyzed. For the olivine and chromite separates, the total analytical blanks for Os constitute less than 0.1%, and for

234 Ir and Ru – less than 0.2% of the total element analyzed. Blank contributions for Re varied between 3% and 12%,

235 for Pt – between 5% and 30%, and for Pd – between 3% and 70%.

236   Osmium isotopic measurements were accomplished via negative thermal ionization mass-spectrometry

237 (NTIMS: Creaser et al., 1991). All samples were analyzed using a secondary electron multiplier (SEM) detector of a

238 *ThermoElectron Triton* mass spectrometer at the *Isotope Geochemistry Laboratory (IGL),* University of Maryland.

239 The measured isotopic ratios were corrected for mass fractionation using ^{192}Os/^{188}Os = 3.083. The internal precision

240 of measured ^{187}Os/^{188}Os in all samples was better than 0.05% (2σ$_{mean}$). The ^{187}Os/^{188}Os of 300 pg loads of the in-

241 house Johnson-Matthey Os standard measured over the course of the entire analytical campaign averaged

242 0.11376±11 (±2σ$_{stdev}$, N = 54). This value characterizes the external precision of the isotopic analysis (0.10%). We

243 used this value to assess the true uncertainty on the measured ^{187}Os/^{188}Os ratio for each individual sample. The

244 ^{187}Os/^{188}Os ratio measured in each sample was also corrected for the instrumental bias relative to the average

245 ^{187}Os/^{188}Os = 0.11378 measured in the Johnson-Matthey Os standard on the Faraday cups of the *IGL Triton*. The

246 correction factor of 1.00018 was calculated by dividing this value by the average ^{187}Os/^{188}Os measured in the

247 Johnson-Matthey Os standard on the SEM of this instrument.

248   The measurements of Ru, Pd, Re, Ir, and Pt were performed at the *IGL* via inductively coupled plasma mass-

249 spectrometry (ICP-MS) using a *Nu Plasma* instrument with a triple electron multiplier configuration in a static

250 mode. Isotopic mass fractionation was monitored and corrected for by interspersal of samples with standards. The

251 accuracy of the data was assessed by comparing the results for the reference materials UB-N and GP-13 obtained

252 during the ongoing analytical campaign. Concentrations of all HSE and Os isotopic compositions obtained at the

253 *IGL* are in good agreement with the results from other laboratories (**Table 1**). Diluted spiked aliquots of iron

254 meteorites were run during each analytical session as secondary standards. The results from these runs agreed within

255 1% for Re and Ir, and within 2% for Ru, Pt, and Pd, with fractionation-corrected values obtained from

256 measurements of undiluted iron meteorite solutions using Faraday cups of the same instrument with signals of >100

257 mV for the minor isotopes. We therefore cite ±1% as uncertainty on the concentrations of Re and Ir, ±2% on the

258 concentrations of Ru, Pt, and Pd, and ±0.1% on the concentrations of Os in the whole-rock samples. For the olivine

259 and chromite separates, the uncertainties on the Os, Ir, and Ru abundances were the same as for the whole-rock

260 samples, whereas the uncertainties on the Re concentrations were between 1.5% and 6%, Pt – between 2.5% and

261 15%, and Pd – between 1.5% and 35%, assuming a ~50% variation in abundances in the total analytical blank

262 (TAB). The uncertainty on the Re concentration was the main source of uncertainty on the Re/Os ratio. For the

263   whole-rock samples, this uncertainty was, thus, estimated to be 1.0%, and for the olivine and chromite separates –

264   between 1.5% and 6%.

265   All regression calculations were performed using ISOPLOT 3.00 (Ludwig, 2003). The uncertainties on the

266   concentrations and isotopic ratios used for the regression calculations are as stated above. The initial γ^{187}Os value

267   was calculated as the per cent deviation of the isotopic composition at the time defined by the isochrons relative to

268   the chondritic reference of Shirey and Walker (1998) at that time.

269   The average chondritic Os isotopic composition at the time defined by the isochrons was calculated using the

270   ^{187}Re decay constant $\lambda = 1.666 \times 10^{-11}$ year^{-1}, an early Solar System initial ^{187}Os/^{188}Os = 0.09531, and ^{187}Re/^{188}Os =

271   0.40186 (Smoliar et al., 1996; Shirey and Walker, 1998).

272   *3.2.2 Pt-Os isotopic data.* In the present study, we followed the methodology developed by Puchtel et al.

273   (2004a) and Puchtel et al. (2005) for determining precise initial ^{186}Os/^{188}Os and ^{187}Os/^{188}Os isotopic compositions in

274   materials requiring corrections for the ingrowth of radiogenic ^{186}Os and ^{187}Os, such as Archean komatiites. This

275   methodology involves high-precision simultaneous determination of ^{186}Os/^{188}Os and ^{187}Os/^{188}Os ratios on un-spiked

276   digestions combined with determination of elemental abundance ratios of Pt, Re, and Os on small aliquots taken

277   from the un-spiked digestions to ensure the representativeness of these ratios for each sample digestion. In order to

278   obtain the amount of Os required for the high-precision measurements of the ^{186}Os/^{188}Os and ^{187}Os/^{188}Os ratios

279   (~100 ng), each sample was digested in 4 to 20 CTs, depending on the Os concentrations in the sample. For the

280   initial un-spiked digestions, ~3 g of sample powder, 9 mL of double-purged, triple-distilled conc. HNO_3, and 6 mL

281   of triple-distilled conc. HCl were placed into a double, internally cleaned, 38 mL Pyrex™ CT chilled to 0°C, sealed

282   and kept in an oven at 270°C for 96 hours. After the digestion was complete, the tubes were chilled and opened, 0.5

283   mL of the acid sample solution from each CT in the batch of 4 CTs representing a single sample digestion were

284   transferred into a 25 mL Pyrex™ CT for precise determination of the Re/Os, Ir/Os (for monitoring potential Os

285   losses during aliquot transfer), and Pt/Os ratios in each sample. Before the transfer procedure, the double, internally

286   cleaned, 25 mL Pyrex™ CT was chilled to 0°C and appropriate amounts of the mixed ^{185}Re-^{190}Os and HSE spikes

287   were added to it, followed by 4 mL of double-purged, triple-distilled conc. HNO_3 and 3 mL of triple-distilled conc.

288   HCl, after the sample solution transfer was completed. The sealed CTs with the spiked sample solutions were kept in

289   the oven at 270°C for 24 h to achieve sample-spike equilibration. After opening the CT, the spiked aliquots were

290   processed using the same procedure utilized in the Re-Os and HSE analysis, except that, without a knowledge of the

291   precise weight of the sample represented by the amount of the transferred solution, only the Re/Os, Pt/Os, and Ir/Os

292   ratios were determined. From the remaining part of the un-spiked acid sample solutions, Os was extracted and

293   purified using the same protocol utilized in the Re-Os study. The Os cuts from the batch of CTs, containing a single

294   sample digestion, were combined into one cut and used for the precise measurements of the ^{186}Os/^{188}Os and

295   ^{187}Os/^{188}Os ratios.

296   Measurements of Re, Os, Pt, and Ir isotopic compositions from the spiked aliquots, for the determination of

297   precise Re/Os, Pt/Os, and Ir/Os ratios, were performed using the same protocol utilized in the Re-Os and HSE study

298   outlined above.

299   The high-precision measurements of the ^{186}Os/^{188}Os and ^{187}Os/^{188}Os ratios were performed by *N-TIMS* in a

300   static mode on a nine Faraday collector *ThermoFinnigan Triton*$^{®}$ mass spectrometer at the *IGL*. Signals of >100

301   mV on mass 234 (^{186}Os^{16}O$_3^-$) and 235 (^{187}Os^{16}O$_3^-$) were generated to reach the maximum in-run precisions for the

302   ^{186}Os/^{188}Os and ^{187}Os/^{188}Os ratios. During each run, between 1400 and 2600 ratios were collected for each sample

303   load, and the in-run uncertainties on the measured ^{186}Os/^{188}Os and ^{187}Os/^{188}Os ratios are quoted as $2\sigma_{mean}$. The

304   possible isobaric interference of ^{186}W^{16}O$_3^-$ on ^{186}Os^{16}O$_3^-$ was assessed by measuring ^{184}Os/^{188}Os (modified if

305   ^{184}W^{16}O$_3^-$ present) and monitoring mass 231 (^{183}W^{16}O$_3^-$) using the electron multiplier. Although a signal of ~3-10

306   cps was normally measured at mass 231, its size in comparison to other potential isotopes of W indicated it was not

307   W, and, therefore, no W corrections were made. Instead, the small signals typically observed at mass 231 are

308   consistent with the expected amount of ^{198}Pt^{16}O^{17}O that is produced from the Pt filaments during ionization. This

309   was indicated from the mass scan profiles from mass 226 (^{194}Pt^{16}O$_2$) to mass 230 (^{198}Pt^{16}O$_2$), that clearly show all of

310   the PtO$_2$ isotopes in their expected proportions in the spectrum, and no evidence for WO$_3$ production at mass 230 or

311   231. The mean of the Johnson-Matthey Os standard runs during the period of data collection was 0.001306±5 for

312   ^{184}Os/^{188}Os, 0.1198454±16 for ^{186}Os/^{188}Os, and 0.113788±13 for ^{187}Os/^{188}Os ($2\sigma_{stdev}$, N = 27). The uncertainty on the

313   ^{186}Os/^{188}Os characterizes the external precision of the isotopic analysis (±14 ppm). We used this value to assess the

314   true uncertainty on the measured ^{186}Os/^{188}Os ratio for each individual sample, and also to calculate the uncertainty

315   on the average initial ^{186}Os/^{188}Os ratios. Since our high-precision ^{186}Os/^{188}Os ratios obtained at the *Johnson Space*

316   *Center* and at *IGL* were previously bias-corrected to a common JM Os standard ^{186}Os/^{188}Os value of 0.1198475

317   (Puchtel et al., 2009b), the ^{186}Os/^{188}Os ratios measured in this study were also bias-corrected to ^{186}Os/^{188}Os =

318   0.1198475 using a correction coefficient of 1.0000177. To calculate the initial ^{186}Os/^{188}Os ratios, the Pt/Os ratios

319   obtained from the spiked runs and the ^{190}Pt decay constant $\lambda = 1.477 \times 10^{-12}$ year^{-1} (Begemann et al., 2001) were

320   used. The initial ε^{186}Os values were calculated as part per 10,000 deviation of the ^{186}Os/^{188}Os ratio in the sample at

321   the time of lava emplacement relative to the chondritic reference of Brandon et al. (2006) at that time using an early

322   Solar System initial ^{186}Os/^{188}Os = 0.1198269 at T = 4567 Ma and ^{190}Pt/^{188}Os = 0.00174.

323

324   ## 4. Results

325   ### *4.1. Re-Os isotopic data*

326   The Re-Os isotopic data for the whole-rock samples and olivine and chromite separates from

327   the Komati and Weltevreden komatiite systems are presented in **Table 2** and plotted on Re-Os

328   isochron diagrams in **Fig. 1**.

329   For the Komati system, the data for 15 whole-rock samples, including two replicates and

330   three averages for the spiked aliquots of the unspiked digestions processed for the Pt-Os study to

331   determine the Re/Os and Pt/Os ratios (marked with (*) in **Table 2**), and four pure olivine and

332   chromite separates, define an errochron (MSWD = 4.7) with a slope corresponding to an age of

333   3484±38 Ma and an initial ^{187}Os/^{188}Os = 0.10335±15 (γ^{187}Os = +0.34±0.15, $2\sigma_{mean}$). Sample

334   BV14, a cumulate from the bottom of flow 11 (see Fig. 1 in Puchtel et al., 2013), which is among

335   the most altered samples, plots to the right of the regression line. Its high Re/Os is only partially

336   supported by the respective ingrowth of ^{187}Os and, as such, is likely due to the late addition of

337   Re. This sample was excluded from the isochron regression calculations.

338   For the Weltevreden system, the data from this study, including four averages of the spiked

339   aliquots of the unspiked digestions (also marked with (*) in **Table 2**), combined with those

340   reported by Connolly et al. (2011), define a precise isochron (MSWD = 0.7) with an age of

341   3263±12 Ma and an initial ^{187}Os/^{188}Os = 0.10442±4 (γ^{187}Os = -0.14±0.04, $2\sigma_{mean}$). This age and

342   the ^{187}Os/^{188}Os initial ratio, albeit derived from a much larger dataset, are identical to those

343   reported by Connolly et al. (2011). Sample SA501-7, collected from the B_1 subzone of flow

344   SA501 (see Fig. 2 in Puchtel et al., 2013), plots to the right of the regression line. For reasons

345   discussed in Connolly et al. (2011), this sample was excluded from the isochron regression

346   calculations.

347

348   *4.2. Pt-Os isotopic data*

349   The Pt-Os isotopic data for the Komati and Weltevreden komatiite systems are presented in

350   **Table 3** and are plotted on Pt-Os isochron diagrams in **Fig. 2**. The three samples analyzed,

351   including one replicate, from the Komati Fm. plot with a very limited spread in the Pt/Os ratios

352   below the 3484 Ma chondritic reference line. The average initial ^{186}Os/^{188}Os ratio, calculated for

353   the emplacement age of 3484 Ma and using the measured $^{190}Pt/^{188}Os$ and $^{186}Os/^{188}Os$ ratios in the

354   individual samples, is 0.1198283±9 (initial $\varepsilon^{186}Os$ = -0.12±0.08, $2\sigma_{mean}$).

355   The four samples analyzed, including one replicate, from the Weltevreden Fm., are also

356   characterized by a limited spread in the Pt/Os ratios, but, unlike the Komati system samples, plot

357   well above the 3263 Ma chondritic reference line. The average initial $^{186}Os/^{188}Os$ ratio,

358   calculated for the emplacement age of 3263 Ma using the measured $^{190}Pt/^{188}Os$ and $^{186}Os/^{188}Os$

359   ratios in the individual samples, is 0.1198330±8 (initial $\varepsilon^{186}Os$ = +0.22±0.07, $2\sigma_{mean}$). The

360   uncertainties on both initial ratios are calculated by dividing the long-term external

361   reproducibility for the $^{186}Os/^{188}Os$ ratio in the in-house Johnson-Matthey Os standard obtained

362   during the analytical campaign (±14 ppm) by the square root of the number of samples analyzed

363   for each komatiite system.

364

365   *4.3. HSE abundance data and compositions of the emplaced komatiite lavas*

366   The abundances of the HSE in the Komati and Weltevreden whole-rock komatiite samples

367   and olivine and chromite separates are presented in **Table 4** and plotted on MgO variation

368   diagrams in **Fig. 3**; the CI chondrite-normalized abundances (using average values for the

369   chondrite Orgueil from Horan et al., 2003) are plotted in **Figs. 4 and 5**.

370   The olivine and chromite separates from the Komati system exhibit similar CI chondrite-

371   normalized patterns with chondritic to slightly sub-chondritic Os/Ir, and enrichments in Os, Ir,

372   and especially Ru, relative to Pt and Pd. The chromite has about two orders of magnitude higher

373   Os, Ir, and Ru, and about an order of magnitude higher Pt and Pd contents, compared to the

374   olivine. These patterns and abundances are generally consistent with experimental studies of

375   HSE partitioning between olivine, chromite and silicate melt (Brenan et al., 2003; Brenan et al.,

376   2005; Brenan et al., 2012).

377   The olivine separates from the Weltevreden system exhibit slightly supra-chondritic Os/Ir

378   ratios and are characterized by about one order of magnitude higher Os and Ir, and a factor of

379   two higher Ru contents, compared to the Komati olivines. This pattern of elevated Os and Ir

380   relative to Ru contents is not consistent with effects predicted for magmatic partitioning behavior

381   of these elements between olivine and silicate melt (Brenan et al., 2003; Brenan et al., 2005), and

382   may indicate the presence of sub-micron-sized inclusions of Os-Ir alloys in the Weltevreden

383   olivine separates.

384   The variations in the Pt and Pd abundances *versus* MgO contents in the whole-rock samples

385   are consistent with the typical incompatible behavior of Pt and Pd during komatiite lava

386   differentiation. The Pt and Pd data for both komatiite systems follow tight trends with negative

387   slopes that pass through the measured respective olivine compositions, indicating that olivine

388   was the only liquidus phase that controlled the concentrations of these elements during

389   differentiation of the Komati and Weltevreden lavas, and, at the same time, providing evidence

390   for the immobile behavior of Pt and Pd during seafloor alteration and metamorphism (**Fig. 3**).

391   The Re data for the whole-rock samples from the Komati system show a great deal of scatter

392   on the Re vs. MgO diagram (**Fig. 3**). As mentioned earlier, sample BV14, which has the highest

393   Re content of all, is the one sample that plots beyond analytical uncertainties off the Re-Os

394   isochron (**Fig. 1**), presumably due to post-emplacement Re enrichment. The rest of the samples,

395   however, plot on the isochron that is consistent with the emplacement age of the lavas. This

396   indicates that the post-magmatic processes that acted on these lavas, e.g., seafloor alteration,

397   were nearly contemporaneous with the lava emplacement, and that the Re-Os system remained

398   closed since then.

399   The Re data for the whole-rock samples from the Weltevreden system, with two exceptions,

400   plot on the well constrained regression line that passes through the measured olivine

401   compositions (**Fig. 3**); one of the exceptions also plots off the Re-Os isochron (**Fig. 1**). Based on

402   this observation, we conclude, also following Connolly et al. (2011), that Re in the Weltevreden

403   system, with the exception of the two samples, displays magmatic behavior and was essentially

404   immobile during seafloor alteration and metamorphism.

405   Among the HSE we analyzed, Re is the most fluid-mobile element; Pd and especially Pt are

406   much less mobile (e.g., Colodner et al., 1992; Puchtel et al., 2007), and Os, Ir, and Ru are even

407   less mobile than Pt. This observation allows us to extend the conclusion regarding the

408   immobility of Pt and Pd, to Os, Ir, and Ru, for both komatiite systems.

409   Variations of the Os and Ir abundances in the Komati and Weltevreden systems show similar

410   patterns, although the magnitude of the variations is a factor of three larger in the latter (**Figs. 3**

411   **and 4**). The upper chilled margin samples from both systems contain ~1.4 ppb Os (and Ir). The

412   spinifex zones show a typical pattern of decreasing Os and Ir abundances with decreasing the

413   MgO contents. The largest range of variations in both systems (e.g., the Os abundances vary

414   between 1.0 and 3.7 ppb in the Komati and between 1.0 and 12.0 ppb in the Weltevereden

415   systems) is observed among olivine cumulate samples with essentially identical MgO contents.

416   Furthermore, there is a general decrease in Os and Ir contents in the upper parts, and an increase

417   in the lower parts of the olivine cumulate zones, relative to those in the chilled margin samples.

418   The olivine separates, on the other hand, are characterized by highly variable Os and Ir contents

419   that are either lower (Komati) or higher (Weltevereden) than those in the chilled margin samples.

420   These observations indicate that the Os and Ir abundances in the cumulate portions of the Komati

421   and Weltevreden komatiite lava flows were not controlled by fractionation of olivine, but rather

422   by an Os-Ir rich phase, such as an Os-Ir alloy. This interpretation was previously put forward for

423   so-called Munro-type komatiitic lavas (Puchtel and Humayun, 2005), i.e., the komatiitic lava

424   flows that exhibit positive correlations between Os, Ir abundances and the MgO contents, as

425   opposed to the Kostomuksha-type lavas, which exhibit negative correlations. The observed

426   pattern of Os and Ir depletions in the upper parts of cumulate zones and enrichments in the lower

427   parts relative to the compositions of the chilled margin samples has been previously documented

428   for some Abitibi komatiite lavas (Puchtel et al., 2004b). This observation lends further support to

429   the notion that olivine does not play a major role in controlling Os and Ir abundances during

430   komatiite lava differentiation (Puchtel and Humayun, 2001; Puchtel et al., 2004b; Barnes and

431   Fiorentini, 2008), and is consistent with the experimental data of Brenan et al. (2005).

432   Ruthenium abundances show minimal variations across the lava flows from both komatiite

433   systems (**Fig. 3**), indicating that the bulk solid-liquid partition coefficient for Ru was close to

434   unity, consistent with trends also established for late Archean komatiite systems (e.g., Puchtel et

435   al., 2004b; Puchtel and Humayun, 2005; Puchtel et al., 2007; Barnes and Fiorentini, 2008). With

436   a few exceptions, samples plot on olivine control lines in Ru *vs*. MgO diagrams (**Fig. 3**),

437   consistent with the notion that variations of Ru abundances in komatiite lavas were controlled

438   largely by fractionation of olivine (Brenan et al., 2003; Barnes and Fiorentini, 2008). Several

439   cumulate samples plot above the olivine control lines (**Fig. 3**). These samples also have

440   somewhat elevated Cr concentrations (Puchtel et al., 2013), which may indicate the presence of

441   small amounts of cumulus chromite with associated platinum-group minerals, as suggested

442   previously (Puchtel and Humayun, 2001; Barnes and Fiorentini, 2008; Brenan et al., 2012).

443   In order to calculate the HSE abundances in the emplaced komatiite lavas, we used the

444   ISOPLOT (Ludwig, 2003) bivariate linear regression analysis, assuming the MgO contents in the

445   emplaced lavas of 29.4±0.4 and 31.4±0.9% for the Komati and Weltevreden systems,

446   respectively (Puchtel et al., 2013); the results are presented in **Table 5**. The projected emplaced

447   lava for the Komati system contained (ppb) 1.3±0.1 Os, 1.4±0.1 Ir, 3.6±0.2 Ru, 4.8±0.4 Pt, and

448   4.7±0.4 Pd, as compared to 1.4±0.1 Os, 1.5±0.1 Ir, 6.3±0.2 Ru, 8.5±0.5 Pt, and 6.6±0.5 Pd for

449   the Weltevreden system. The Re content in the Weltevreden emplaced lava is calculated to be

450   0.33±0.03 ppb, whereas Re content in the Komati emplaced lava cannot be calculated due to

451   post-eruption mobility of Re. The emplaced lavas from the Komati and Weltevreden systems,

452   thus, had chondritic to slightly sub-chondritic CI-normalized $Os/Ir_N = 0.93\pm0.05$ and 0.94±0.08,

453   respectively, and similarly moderately fractionated HSE patterns ($Pd/Ir_N = 2.7\pm0.2$ and 3.5±0.2,

454   respectively). The absolute Ru and Pd abundances are ~50% higher and Pt abundances were

455   about a factor of two higher in the emplaced Weltevreden lava compared to its Komati

456   counterpart (**Fig. 4**). This indicates significant Pt enrichment, compared to the HSE with similar

457   compatibility, such as Pd, in the Weltevreden system.

458

459   **5. Discussion**

460   *5.1. Absolute and relative HSE abundances in the sources of the Komati and Weltevreden*

461   *komatiite systems*

462   The Re-Os and Pt-Os isotopic systems are partially or wholly governed by the strong

463   partitioning of these elements into metal or sulfide liquid, relative to silicate melt. Additionally,

464   during mantle melting, Os is typically compatible with the melting residue, whereas Pt and Re

465   are incompatible (Barnes et al., 1985; Rehkämper et al., 1999b). The Re-Os and Pt-Os isotopic

18

466 systems, therefore, provide valuable insights into certain processes, to which the more

467 traditional, lithophile element-based isotopic systems, are less sensitive. These processes include

468 planetary accretion and mantle/core differentiation.

469 The initial $^{186}Os/^{188}Os$ and $^{187}Os/^{188}Os$ ratios obtained in the Pt-Os and Re-Os isotopic studies

470 of a range of mantle-derived materials provide measures of long-term evolution of Pt/Os and

471 Re/Os in the mantle. These studies to-date have produced a remarkably variable array of data

472 that has been used to constrain Re-Os and Pt-Os isotopic parameters of major mantle reservoirs

473 (see review in Walker (2009) and references therein), such as the putative Primitive Mantle (PM)

474 and Depleted MORB Mantle (DMM). The evolution trajectories for current estimates of these

475 major reservoirs are plotted in **Fig. 6** and are further used as reference parameters.

476 The modern Os isotopic composition of the PM, i.e., hypothetical mantle reservoir that has

477 not experienced melt depletion, has been constrained on the basis of studies of global suites of

478 mantle xenoliths ($\gamma^{187}Os$ = +2.04±0.63: Meisel et al., 2001), as well as Os-rich alloys ($\varepsilon^{186}Os$ =

479 +0.10±0.13: Walker et al., 2005; Brandon et al., 2006).

480 The Os isotopic composition of the DMM, or modern convecting upper mantle that has lost

481 melt due to extraction of oceanic crust, is a controversial issue, with as much as a ~3% difference

482 in average $^{187}Os/^{188}Os$ obtained from abyssal peridotites (Snow and Reisberg, 1995; Brandon et

483 al., 2000; Liu et al., 2009) compared with estimates based on projections to the present from

484 Proterozoic and Phanerozoic ophiolites (Walker et al., 1996; Tsuru et al., 2000; Walker et al.,

485 2002). The $\gamma^{187}Os$ value of the DMM, based on data compiled for abyssal peridotites, is -1.40

486 ±0.93 (Snow and Reisberg, 1995; Brandon et al., 2000; Liu et al., 2009). In comparison, the

487 $\varepsilon^{186}Os$ value of DMM, based on a still limited data for abyssal peridotites (Brandon et al., 2000),

488 is -0.27±0.07 ($2\sigma_{mean}$).

489   Here, we use the initial $^{186}Os/^{188}Os$ and $^{187}Os/^{188}Os$ ratios obtained for the Komati and

490   Weltevreden systems as a measure of long-term evolution of Pt/Os and Re/Os in the early

491   Archean mantle sources of these komatiite systems. In order to constrain the long-term source

492   characteristics, we calculate the parent/daughter elemental ratios necessary to achieve isotopic

493   compositions at the times of komatiite formation by initially assuming formation of the mantle

494   domains at the time of Solar System formation. It is calculated that the Komati source would

495   have evolved from early Solar System initial ratios for $^{186}Os/^{188}Os = 0.1198269$ at 4.567 Ga

496   (Brandon et al., 2006) and $^{187}Os/^{188}Os = 0.09531$ at 4.558 Ga (Shirey and Walker, 1998), to the

497   komatiite initial $^{186}Os/^{188}Os = 0.1198283\pm9$ and $^{187}Os/^{188}Os = 0.10334\pm8$ at 3484 Ma, with time-

498   integrated $^{190}Pt/^{188}Os = 0.00085\pm56$ and $^{187}Re/^{188}Os = 0.419\pm4$. The Weltevreden source would

499   have evolved to its initial $^{186}Os/^{188}Os = 0.1198330\pm8$ and $^{187}Os/^{188}Os = 0.10442\pm4$ at 3263 Ma

500   with time-integrated $^{190}Pt/^{188}Os = 0.00312\pm41$ and $^{187}Re/^{188}Os = 0.396\pm2$. Although the time-

501   integrated $^{187}Re/^{188}Os$ in both sources are similar to the chondritic reference value of 0.402

502   (Shirey and Walker, 1998), the $^{190}Pt/^{188}Os$ are non-chondritic. For the Komati system, the

503    $^{190}Pt/^{188}Os$ is subchondritic. When the full uncertainty on the calculated $^{190}Pt/^{188}Os$ in the Komati

504   system is considered (±0.00056), the highest value permitted by the uncertainty (0.00141) is still

505   ~12% lower than the lowest $^{190}Pt/^{188}Os$ recorded in any group of chondrites (the average values

506   are 0.00177 ± 20, 0.00175 ± 16, and 0.00178 ± 11 ($2\sigma_{stdev}$) in carbonaceous, ordinary, and enstatite

507   chondrites, respectively, as compiled from data of Horan et al. (2003) and Brandon et al.

508   (2005a)).

509   For the Weltevreden system, the calculated $^{190}Pt/^{188}Os$ of its source is suprachondritic. When

510   the full uncertainty on the calculated $^{190}Pt/^{188}Os$ in the Weltevreden source is considered

511   (±0.00041), the lowest value permitted by the uncertainty (0.00271) is 40% higher than the

512   highest $^{190}Pt/^{188}Os$ recorded in any group of chondrites. In reality, the reservoirs that the Komati

513   and Weltevreden system komatiites were derived from likely formed sometime after Solar

514   System formation, so the requisite Pt/Os ratios in the sources of both systems would have to have

515   been even more fractionated from the chondritic reference. This will be discussed in the

516   following sections.

517   It is well established that in the mantle, the platinum-group elements (PGE) are largely

518   hosted by sulfides and/or by PGE alloys (Barnes et al., 1985; Lorand et al., 1999; Rehkämper et

519   al., 1999b; Lorand and Alard, 2001; Luguet et al., 2007), whereas Re resides in both silicates and

520   sulfides (Reisberg and Lorand, 1995; Fonseca et al., 2007; Brenan, 2008). There are two

521   principal types of sulfides in the mantle – high-temperature monosulfide solid solution, Mss, that

522   usually occurs as inclusions in silicates, mostly in olivine, and the lower-temperature Cu-Ni-rich

523   sulfides, that are usually interstitial to major silicate minerals (Luguet et al., 2007). The Mss

524   preferentially accommodates Os, Ir, and Ru, whereas the Cu-Ni-rich sulfides preferentially host

525   Pt, Pd, and Re. Osmium-Ir-Ru alloys are usually residual phases remaining and/or forming in

526   refractory mantle peridotites (e.g., harzburgites) in response to consumption of sulfides during

527   high-degrees (>25%) partial melting (Keays, 1995; Luguet et al., 2007).

528   In order to calculate the absolute abundances of the HSE in the sources of the Komati and

529   Weltevreden komatiite systems, we use the technique that has been previously developed and

530   applied in studies of other komatiite systems (e.g., Puchtel et al., 2004b; Puchtel and Humayun,

531   2005). This technique is based on the assumption that an element behaves similarly during both

532   partial melting in the mantle source and fractional crystallization of the erupted lava. Thus, if an

533   HSE was incompatible with the liquidus mineral assemblage during differentiation of an

534   emplaced komatiite lava, it was also likely similarly incompatible with the residual mineral

535   assemblage during melting that produced the lava. For a specific komatiite lava suite, the

536   abundances of elements that are incompatible with the melting residue (i.e., the mineral hosts of

537   these elements have been exhausted during melting) should plot on the liquid lines of descent.

538   The latter can be established via regressing the abundances of the incompatible elements vs.

539   MgO contents in the lavas. The source concentrations of the incompatible elements can then be

540   calculated via projecting the abundances in the lavas to the assumed MgO content in the source

541   (the so-called projection technique). Since the MgO content of the mantle is little affected by

542   variations in the degree of previous melt extractions, Puchtel et al. (2004b) used the average

543   MgO content of 38% for depleted spinel peridotites sampled worldwide, which is also the

544   accepted value for the putative PM (McDonough and Sun, 1995).

545   It should be noted, however, that the sulfur content at saturation of a mafic magma increases

546   with decreasing pressure, so magmas may become undersaturated during adiabatic ascent

547   (Mavrogenes and O'Neill, 1999). As a result, the bulk HSE partition coefficients of the first

548   phases to fractionate could differ from those that last enter the melt during partial melting. This

549   limitation can only be relaxed if there are no sulfides left in the source after melt separates from

550   the residue. Therefore, one of prerequisites for this methodology to be applicable for calculating

551   the HSE composition of a mantle source of lavas from their HSE abundances is the complete

552   exhaustion of low-temperature Cu-Ni-rich sulfides in the source during partial melting. This can

553   only be attained if the degree of melting exceeds ~30% (Barnes et al., 1985; Keays, 1995;

554   Rehkämper et al., 1999b); this degree of melting is typical of komatiite formation.

555   The assumption of complete exhaustion of Cu-Ni-rich sulfides in the sources can be tested

556   against the behavior of PGE that are largely controlled by these sulfides during melting and

557   differentiation. Compatible behavior of Pt and Pd, as well as chalcophile elements, such as Cu,

558   Zn, and Ga, during lava differentiation is normally associated with sulfide-saturated conditions,

559   such as those that obtained during formation of lower degree melts, e.g., MORB (Hamlyn et al.,

560   1985; Peach et al., 1990; Bezos et al., 2005). By contrast, the observation that Pt and Pd, as well

561   as chalcophile elements Ga and Zn (Puchtel et al., 2013), behaved strongly incompatibly during

562   differentiation of both Komati and Weltevreden lavas (**Fig. 3**), provides strong evidence that

563   these two komatiite systems were sulfide-undersaturated upon lava emplacement. This is an

564   important observation that also indicates that both the Komati and Weltevreden komatiite

565   magmas did not undergo sulfide liquid fractionation prior to emplacement, and, thus, their HSE

566   inventories were likely preserved *en route* from mantle source to surface eruption.

567   In order to estimate the abundances of the incompatible HSE (Re, Pt, and Pd) in the Komati

568   and Weltevreden sources, we project the abundances of these elements measured in the lavas and

569   in the olivine separates for each of the two komatiite systems to MgO = 38 wt%. The resulting

570   projected source abundances are presented in **Table 5**. The concentrations of Pt calculated by

571   means of ISOPLOT-regression of data for both whole-rock samples and olivine separates, are

572   2.9 ± 0.2 ppb and 6.0 ± 0.4 ppb, and for Pd are 2.9 ± 0.2 ppb and 4.6 ± 0.3 ppb ($2\sigma_{mean}$) in the Komati

573   and Weltevreden sources, respectively. The Re abundance in the source of the Weltevreden

574   system is calculated to be 0.23 ± 0.02 ppb ($2\sigma_{mean}$). Due to evidence for post-eruption mobility of

575   Re in the Komati lavas, its abundance in the Komati source cannot be calculated directly using

576   this technique, but is estimated using the Os isotopic data, below.

577   To calculate the Ru abundances in the sources, we used the observation that olivine

578   fractionation was the main control on the variations of Ru abundances in both systems. As such,

579   we used the linear regressions of Ru vs. MgO in **Fig. 3** to obtain Ru abundances in the sources of

580   the Komati and Weltevreden systems to be 3.5 ± 0.3 ppb and 6.0 ± 0.3 ppb, respectively.

581   The observed compatible behavior of Os and Ir during lava differentiation indicates that the

582   emplaced lavas were saturated with respect to the hosts of these elements. As such,

583   concentrations of Os and Ir in the sources of the Weltevreden and Komati lavas cannot be

584   calculated directly using the projection technique. The Os contents must be estimated indirectly

585   using the calculated Pt (for the Komati system) and Re (for the Weltevreden system) abundances

586   in their sources, and the time-integrated $^{190}Pt/^{188}Os$ and $^{187}Re/^{188}Os$ derived from the initial

587    $^{186}Os/^{188}Os$ and $^{187}Os/^{188}Os$ for the Komati and Weltevreden systems, respectively, using the

588   following equations:

589

590        $Os = Pt/(1047 \times ^{190}Pt/^{188}Os)$, $Os = Re/(0.2115 \times ^{187}Re/^{188}Os)$ (1)

591        $^{190}Pt/^{188}Os = (^{186}Os/^{188}Os_i - 0.1198269)/(\exp(\lambda_1 \times 4.567) - \exp(\lambda_1 \times T))$ (2)

592        $^{187}Re/^{188}Os = (^{187}Os/^{188}Os_i - 0.09531)/(\exp(\lambda_2 \times 4.558) - \exp(\lambda_2 \times T))$ (3)

593

594   where i denotes the respective Os initial isotopic ratio calculated for the time of the lava

595   emplacement T, and λ_1 and λ_2 are decay constants of ^{190}Pt and ^{187}Re, respectively. The

596   uncertainties on the Os concentrations are derived from the uncertainties on the initial Os

597   isotopic compositions and on the calculated Pt and Re concentrations. The uncertainties on the

598   Os abundances derived from (2) are relatively large compared to those calculated from (3).

599   The calculated time-integrated Os concentrations are 3.3±1.1 ppb and 2.7±0.2 ppb for the

600   Komati and Weltevreden systems, respectively. The time-integrated Re content in the Komati

601   source is then calculated to be 0.29±0.10 ppb. The Ir abundances in the sources are calculated

602   using the Os contents and the Os/Ir in the emplaced komatiite lavas on the basis of the

603   observation that during high-degree partial melting, komatiite melts mimic the Os/Ir ratios of

24

604   their mantle sources due to complete exhaustion of low-temperature Cu-Ni sulfides and Os-Ir

605   alloy saturation in the former (Fonseca et al., 2011; Fonseca et al., 2012). The calculated Ir

606   contents are 3.5±1.2 ppb and 3.0±0.3 ppb in the Komati and Weltevreden komatiite systems,

607   respectively.

608

609   *5.2. The origin of the absolute and relative HSE abundances in the sources of the Komati*

610   *and Weltevreden komatiite systems*

611   As is evident from **Fig. 6**, the sources of Archean komatiite systems, as well as 3.81 Ga

612   peridotites from Isua (Bennett et al., 2002), are characterized by initial $^{187}Os/^{188}Os$ that are

613   identical, within the uncertainty, to the chondritic reference of Shirey and Walker (1998), with

614   initial $\gamma^{187}Os$ values ranging, with two exceptions (the 2.8 Ga Kostomuksha and 3.55 Ga

615   Schapenburg systems), only from -0.1 to +0.4 (**Fig. 6**). These nearly uniform initial ratios are

616   difficult to place in the context of the evolution trajectories for contemporary mantle reservoirs

617   presented in **Fig. 6**, as the initial Os isotopic compositions of the komatiite sources lie largely

618   below the $\gamma^{187}Os$ evolution trajectory of the putative PM, yet well above the evolution trajectory

619   for the contemporary DMM, as based on abyssal peridotites. One explanation might be that these

620   komatiite systems were derived from lower mantle sources, with Os isotopic evolution different

621   from that of the oceanic mantle, as would be expected if they were generated within plumes

622   rising from the lower mantle. Consistent with this, there is strong petrologic/geochemical

623   evidence for a plume origin for both the Komati and Weltevreden komatiites (Puchtel et al.,

624   2013), as well as for most other komatiite systems presented in **Fig. 6** (Campbell et al., 1989;

625   Puchtel et al., 1997; Puchtel et al., 1998; Puchtel et al., 1999; Puchtel et al., 2009a; Puchtel et al.,

626   2009b). As such, the sources of these komatiites may have had distinct, lower mantle HSE

627 characteristics, as was also proposed by studies that involved a combination of ^{182}W – ^{186,187}Os

628 (Touboul et al., 2012) and ^{142,143}Nd – Lu-Hf (Puchtel et al., 2013) isotopic systems.

629 The limited dataset of initial ^{186}Os/^{188}Os ratios that has been generated for komatiite systems

630 indicate that mantle sources of two late Archean systems, Abitibi and Belingwe (Puchtel et al.,

631 2004a; Puchtel et al., 2009b) evolved with time-integrated Pt/Os within the chondritic range. The

632 high initial ^{186}Os/^{188}Os and ^{187}Os/^{188}Os of the mantle source of the 2.8 Ga Kostomuksha

633 komatiites, however, requires an enriched, long-term suprachondritic Pt/Os and Re/Os (Puchtel

634 et al., 2005).

635 Of the two early Archean komatiite systems examined here, the Komati system evolved with

636 time-integrated Pt/Os that was below the chondritic value. By contrast, the Weltevreden source

637 evidently evolved with a strongly supra-chondritic Pt/Os ratio. Despite the difference in initial

638 ^{186}Os/^{188}Os, the time-integrated Re/Os for both komatiite systems are well within the range of

639 those in chondrites.

640 Next, we consider the types of processes that could have caused such types of fractionations.

641 These cannot be either core-mantle interaction (Walker et al., 1995; Walker et al., 1997; Brandon

642 et al., 1998; Brandon and Walker, 2005; Humayun, 2011) or oceanic lithosphere recycling

643 (Walker et al., 1991; Lassiter and Hauri, 1998), as both processes should result in long-term

644 coupled enrichments in Re/Os and Pt/Os, albeit to a different relative degree.

645 The long-term fractionations of Pt/Os observed in the sources of the Komati and

646 Weltevreden komatiite systems must have occurred very early in Earth history, as required by

647 the ages of the komatiites, coupled with the length of time required to grow the observed

648 ^{186}Os/^{188}Os isotopic anomalies. Recently, based on the results of lithophile trace element and

649 ^{142,143}Nd and Lu-Hf isotope studies, (Puchtel et al., 2013) argued that both the Komati and

650   Weltevreden komatiites were derived from mantle domains that formed as late as 4400 Ma, as a

651   result of crystallization of a primordial magma ocean, with Mg-perovskite and minor Ca-

652   perovskite acting as fractionating mineral phases. The Pt/Os fractionation inferred for the source

653   of the Weltevreden komatiite system, as well as the less pronounced fractionation likely required

654   for the Komati source, could also be the result of such primordial differentiation, although the

655   mechanisms involved, due to the contrasting behaviors of the lithophile and highly siderophile

656   parent and daughter elements during planetary differentiation, must be different.

657   Recently, on the basis of combined ^{182}W and ^{186,187}Os isotopic data, Touboul et al. (2012)

658   argued that the mantle source of the 2.8 Ga Kostomuksha komatiite system included material

659   from a primordial reservoir that represented either a deep mantle region that underwent metal-

660   silicate equilibration, or a product of large-scale magmatic differentiation of the mantle. The

661   short-lived nature of the ^{182}Hf-^{182}W system ($t_{1/2}$ ~9 Ma) requires that the isotopically anomalous

662   reservoir formed within the first 30 million years of Solar System history. These authors also

663   concluded that the preservation of this reservoir, until at least 2.8 billion years ago, is strong

664   evidence for sluggish mixing of at least some portions of the mantle throughout the Hadean and

665   Archean. The mantle domains that preserved the ^{143}Nd and ^{176}Hf memory of an early mantle

666   differentiation event and ultimately gave rise to the Komati and Weltevreden komatiite sources

667   (Puchtel et al., 2013), may also have preserved the Re-Os and Pt-Os memory of this event. The

668   question that remains, then, is the nature of the mechanism that was responsible for the

669   fractionation of the Pt/Os in the sources of these komatiites, but did not detectably affect the

670   Re/Os. The process that holds the key to the lithophile element differentiation may provide some

671   clues to the HSE differentiation as well.

672   It has been shown by several authors that Mg-perovskite, the dominant lower mantle mineral,

673   has a strong affinity for Fe_2O_3; the latter is so strong that its Fe^{3+} content is independent of

674   oxygen fugacity (Frost et al., 2004; Wade and Wood, 2005; Frost et al., 2008). High levels of

675   Fe^{3+} are present in perovskite, even when it is in chemical equilibrium with metallic iron. Since

676   the lower mantle must have been poor in Fe_2O_3 during core formation, FeO would have

677   disproportionated to produce Fe_2O_3 to form Mg-perovskite and iron metal. Frost et al. (2004) and

678   Frost and McCammon (2008) argue that, following crystallization of a putative magma ocean,

679   the lower mantle must have contained approximately 1 wt% of a metallic iron-rich alloy. The

680   fate of this iron alloy is not clear. Wade and Wood (2005) and Frost et al. (2008) suggest that the

681   loss of some of this iron metal to the core is required to bring the oxidation state of the mantle to

682   its present levels. The dispersal of the residual iron metal in the lower mantle, as might have

683   occurred via magma ocean crystallization and/or overturn, might also have facilitated the

684   fractionation of Pt from other HSE in some lower mantle domains.

685   Experimental data indicate that, under the reducing conditions expected during crystallization

686   of a primordial magma ocean (Frost et al., 2008), Pt has strong tendency to form Fe-Pt alloys

687   (Borisov and Palme, 1997, , 2000). This tendency is much less for Pd and essentially does not

688   occur for the other HSE. Some portion of the iron metal that formed as a result of

689   disproportionation of FeO during crystallization of Mg-perovskite at the bottom of a magma

690   ocean might have combined with Pt to form Fe-Pt alloys. Dispersal of Fe-Pt alloys to lower

691   mantle domains could have resulted in the creation of Pt-enriched and Pt-depleted domains. The

692   enrichments and depletions would not necessarily correlate with enrichments and depletions in

693   the other HSE, so high- and low Pt/Os domains may have been created. Such a scenario can

694   potentially explain the observed time-integrated non-chondritic Pt/Os, coupled with the

695   chondritic Re/Os, in the sources of the Komati and Weltevreden komatiite systems. This

696   fractionation must have occurred simultaneously with the major silicate differentiation

697   established on the basis of the ^{142,143}Nd-^{176}Hf isotopic study (Puchtel et al., 2013), i.e., as late as

698   4400 Ma, and the mantle reservoirs sampled by the Weltevreden lavas must have remained

699   isolated from the rest of the mantle not only in terms of the lithophile element (Puchtel et al.,

700   2013), but also in terms of the Re-Pt-Os isotope systematics.

701   Assuming that our conclusions about the nature of the Pt/Os fractionation in the sources of

702   the Komati and Weltevreden systems are correct, we can calculate the original Pt abundances

703   that existed in the sources of both systems prior to the 4400 Ma differentiation event. Since both

704   sources are characterized by chondritic initial ^{187}Os/^{188}Os, and, thus, evolved with time-

705   integrated chondritic ^{187}Re/^{188}Os ratios, it is logical to assume that their initial ^{186}Os/^{188}Os ratios

706   prior to the major silicate differentiation event (4400 Ma) were also chondritic, and, thus, these

707   systems evolved up to that point in time with chondritic ^{190}Pt/^{188}Os. As such, we solve equations

708   (1-3) for Pt, using the Os concentrations calculated from the Pt-Os (Komati: 3.3±1.1 ppb Os) and

709   Re-Os (Weltevreden: 2.7±0.2 ppb Os) isotopic data and assuming chondritic evolution to 4400

710   Ma. Our calculations yield the Pt abundances of 5.9±0.9 ppb and 4.9±0.7 ppb in the sources of

711   the Komati and Weltevreden komatiite systems, respectively, with the uncertainties defined by

712   both the uncertainties on the initial ^{186}Os/^{188}Os isotopic compositions and on the calculated Os

713   abundances.

714   The HSE concentrations in the Komati and Weltevreden komatiite sources, calculated using

715   the assumptions discussed above (**Table 5),** are plotted as CI chondrite-normalized abundances

716   in **Fig. 7**, together with an estimate of average HSE abundances in the sources of late Archean

717   komatiite systems compiled on the basis of data of Puchtel et al. (2004a; 2004b; 2007, 2009b)

718   and Puchtel and Humayun (2005). These data are compared with the HSE abundances estimated

719   for the modern PM of Becker et al. (2006).

720   The CI chondrite-normalized abundances in the sources of the two komatiite systems display

721   contrasting, differently fractionated patterns. The Komati system source is depleted in Pt and Pd

722   relative to Os and Ir (Pd/Ir$_N$ = 0.83±0.29), whereas the Weltevreden system source is enriched in

723   Pt and Pd over Os and Ir (Pd/Ir$_N$ = 1.6±0.1). Interestingly, the combined Komati-Weltevreden

724   komatiite system source, calculated as an average of the HSE abundances present in the two

725   sources, exhibit near-chondritic CI chondrite-normalized HSE patterns, with Pd/Ir$_N$ = 1.2.

726   In **Fig. 8**, the calculated absolute abundances of HSE in the sources of the Komati and

727   Weltevreden komatiite systems are plotted as a function of age and are compared with the HSE

728   abundances in the sources of late Archean komatiite systems and in the estimate of the modern

729   PM. Since, out of all HSE, Pt and Pd (and Re, where post-emplacement mobility was not an

730   issue) are determined with the highest degree of confidence for all komatiite systems, only the

731   total concentrations of Pt and Pd are plotted and compared. In the calculations of the totals, the

732   relative weight of the Pd contribution to the total was normalized to that of Pt on the basis of

733   their relative abundances in an average CI chondrite Orgueil (Horan et al., 2003) using 1.52 as a

734   normalizing coefficient.

735   The first observation evident from **Fig. 8** is that the total Pt+Pd abundances in the sources of

736   the near-contemporaneous late Archean komatiite systems span a substantial range, from as little

737   as 58±7% in the 2.69 Ga Belingwe system to as much 85±5% in the 2.72 Ga Abitibi system, of

738   the total Pt and Pd present in the estimates for the modern PM. The uncertainty on the total Pt

739   and Pd abundances in the latter are such that the total Pt and Pd abundances in some late Archean

740   komatiite systems, e.g., Abitibi and Kostomuksha, overlap with those in the estimates for the

741   PM, whereas others (Vetreny, Belingwe, Volotsk-Kenozero) do not. The second observation is

742   that the total Pt and Pd abundances in the sources of the early Archean komatiite systems are

743   within the range of those in the late Archean komatiite systems, albeit on the lower side, varying

744   from 56±12% for the Komati to 65±10% for the Weltevreden, of the total Pt and Pd present in

745   the estimates for the modern PM. In the next section, we discuss the implications of our results

746   for the evolution of the HSE in the Archean mantle.

747

748   *5.3. Constraints on the origin of absolute and relative HSE abundances in the Archean*

749   *mantle*

750   The observations that the HSE occur in roughly chondritic relative proportions in the upper

751   mantle (Morgan, 1985), and that absolute HSE abundances are two- to four orders of magnitude

752   higher than might be expected based on the low-pressure metal-silicate partitioning data (Morgan

753   et al., 1981) has led to the concept of late accretion. Late accretion is defined for HSE as the

754   addition of ~0.5 wt.% of the mass of the Earth to the mantle after the last major equilibration

755   between the core and mantle (Kimura et al., 1974; Chou et al., 1983). Issues related to late

756   accretion are highly debated, including the time frame within which the bulk of late accreted

757   materials was delivered to Earth, the composition of the late accreted materials, as well as the

758   time frame within which the late accreted materials were homogenized within the mantle. Some

759   of the uncertainties relating to this issue stem from the fact that both the relative and absolute

760   HSE abundances in the Archean mantle are not well constrained, and the causes of apparent

761   variations in the abundances of HSE in the early-Earth mantle are not well understood (see

762   review in Walker (2009) and references therein). For example, on the basis of studies of 3.82 Ga

763   peridotites from West Greenland and 3.46 Ga komatiites from Western Australia, Bennett et al.

764   (2002) concluded that any HSE-rich components added to the mantle by late accretion must have

765   been transported into and grossly homogenized within the mantle by 3.8 Ga. In contrast to these

766   conclusions, Maier et al. (2009) and Fiorentini et al. (2010), on the basis of their studies of Pt

767   contents in komatiitic lavas of various ages, argued for a gradual increase in the HSE abundances

768   in the terrestrial mantle from ~3.5 to ~2.9 Ga, with little change since ~2.9 Ga. They attributed

769   this increase to the slow, downward mixing of a late veneer of chondritic impactors.

770   Our present results, considered together with the data for the late Archean komatiite systems

771   compiled from Puchtel and Humayun (2001, 2005), Puchtel et al. (2004a; 2004b), Puchtel et al.

772   (2005), Puchtel et al. (2007) and Puchtel et al. (2009b), indicate that the calculated total absolute

773   Pt and Pd abundances in the Archean mantle sources sampled by komatiites changed little from

774   3.5 to 2.7 Ga. The one exception, according to our work (Puchtel et al., 2009a), is the 3.55 Ga

775   Schapenburg komatiite system, for which only 27±4% of the total Pt and Pd abundance estimates

776   for the modern PM are calculated. Puchtel et al. (2009a) proposed that the HSE systematics for

777   this komatiite system may have not been set entirely by the addition of chondritic materials after

778   the last major equilibration between the core and the mantle, but also by high-pressure metal-

779   silicate equilibration. A Pt-Os isotopic study of the Schapenburg komatiite system is currently

780   underway and should help clarify this issue.

781   There are several possible reasons for the discrepancy between our observations and

782   conclusions reached by Maier et al. (2009). First, there is a substantial discrepancy in the

783   absolute concentrations of HSE in sample sets from the localities analyzed here and by Maier et

784   al. (2009). Maier et al. (2009) reported Pt contents, re-calculated for 25% MgO, of ~4.5 ppb and

785   ~7.4 ppb and Ru contents of 2.5 ppb and 4.7 ppb for lavas from the Komati and Weltevreden

786   systems, respectively, whereas the data presented here, when also re-calculated for 25% MgO,

787   indicate ~6.0 and ~11.2 ppb and 3.8 and 6.0 ppb, respectively, as can be seen in **Fig. 3**. We can

788   offer no definitive explanation for this discrepancy at this time, but speculate that it could relate

789   to the differences in analytical methods used or preservation of samples analyzed.

790   Second, of all HSE, Pt and Pd (and Re, where not affected by post-magmatic element

791   mobility) are the elements for which the most robust, and most crucial, source estimates can be

792   obtained. In this study, we show that Pt may have been removed from the sources of some early

793   Archean lavas and added to the sources of others very early in Earth history. Indeed, our study

794   reveals long-term Pt-fractionated nature of the sources of the early Archean komatiite systems

795   compared to their late Archean counterparts (**Fig. 7**), which can greatly affect estimates for the Pt

796   abundances in early Archean komatiite sources.

797   Our results allow us to place additional constraints on the timing of the late accretion. Based

798   on the calculated HSE abundances in the sources of the Komati and Weltevreden systems, these

799   contained between 60 and 70% of the late accreted material complement present in the estimates

800   for the modern PM, and about as much as is present in the sources of some late Archean

801   komatiite systems. If our model is correct and the ^{186}Os/^{188}Os isotopic anomalies present in the

802   sources of the early Archean komatiite systems are the result of early differentiation during the

803   solidification of a primordial magma ocean, then most late accreted material must have been

804   added to and homogenized within the mantle before its solidification, e.g., no later than 4400

805   Ma. This conclusion is consistent with both the ^{182}W isotopic data for the Komati system

806   reported by Touboul et al. (2012), as well as with the coupled ^{182}W-HSE data for the

807   Kostomuksha system that require that the bulk of the late accreted materials were added to and

808   homogenized within the mantle within the first 60 Ma of Earth's history (Touboul et al., 2012).

809

Conclusions

Due to their unique properties not found in many terrestrial materials, komatiites are a powerful tool for studies of early-Earth processes. In this study, we report Pt-Re-Os isotopic and HSE abundance data for well preserved komatiites from the 3.48 Ga Komati and 3.26 Ga Weltevreden Fms. of the Barberton Greenstone Belt in South Africa. The Re-Os data for whole-rock samples and pure olivine and chromite separates yield isochrons with ages of 3484±38 and 3263±12 Ma that are consistent with the accepted respective emplacement ages of the Komati and Weltevreden Fms. The calculated initial $^{187}Os/^{188}Os = 0.10335±15$ ($\gamma^{187}Os = +0.34±0.15$) and 0.10442±4 ($\gamma^{187}Os = -0.14±0.04$) for the Komati and Weltevreden systems, respectively, are within the chondritic range. When considered together with the Re-Os data for late Archean komatiite systems, our data indicate that Archean mantle evolved with essentially chondritic time-integrated Re/Os. In constrast, the initial $^{186}Os/^{188}Os = 0.1198283±9$ ($\varepsilon^{186}Os = -0.12±0.08$) and 0.1198330±8 ($\varepsilon^{186}Os = +0.22±0.07$) for the Komati and Weltevreden systems, respectively, are non-chondritic, indicating that mantle sources of these komatiites evolved with fractionated time-integrated Pt/Os.

Our new $^{186,187}Os$ isotopic data for the early Archean komatiite systems, combined with the $^{142,143}Nd$ and ^{176}Hf isotopic data of Puchtel et al. (2013), are consistent with formation, followed by long-term isolation, of deep-seated mantle domains with fractionated time-integrated Sm/Nd, Lu/Hf, and Pt/Os ratios, at ca. 4400 Ma. These domains were likely generated as a result of crystallization of a primordial magma ocean, with Mg-perovskite, Ca-perovskite, and Fe-Pt alloy acting as the fractionating phases. The inferred mantle domains remained isolated from the convecting mantle for at least 1.3 billion years, but were largely mixed away by 2.7 Ga on the scale of mantle reservoirs sampled by late Archean komatiite lavas emplaced worldwide, as evidenced by uniform time-integrated Sm/Nd, Lu/Hf, and Pt/Os ratios in late Archean komatiite systems.

The total Pt and Pd abundances in the sources of early Archean komatiite systems, corrected for the inferred Pt fractionation during crystallization of the terrestrial magma ocean, are calculated to be between 60% and 70% of those present in estimates for the modern PM. These are within the range of the total HSE abundances present in the sources of late Archean komatiite systems, indicating little change in HSE abundances in the Archean mantle between 3.5 and 2.7 Ga.

841   Higher Pt abundances in late Archean komatiites, compared to their early Archean

842   counterparts, have been taken as evidence for sluggish, downward mixing of late accreted

843   material into the mantle (Maier et al., 2009; Fiorentini et al., 2011). Our new isotopic and HSE

844   abundance data for early Archean komatiite systems are inconsistent with such a scenario.

845   Instead, our data require that late accretion of HSE to Earth was largely complete by the time the

846   terrestrial magma ocean had crystallized. Rather than downward mixing of an HSE-rich late

847   veneer, the Pt concentration variations observed in early Archean komatiites may reflect sluggish

848   mixing of diverse post-magma ocean domains characterized by variably fractionated both

849   lithophile element and HSE abundances.

850

Acknowledgements

855

References

Alves, S., Schiano, P., Allegre, C.J., 1999. Rhenium-osmium isotopic investigation of Java subduction zone lavas. Earth and Planetary Science Letters 168 (1-2), 65-77.

Armstrong, R.A., Compston, W., DeWit, M.J., Williams, I.S., 1990. The stratigraphy of the 3.5-3.2 Ga Barberton greenstone belt revisited: A single zircon ion microprobe study. Earth and Planetary Science Letterrs 101 (1), 90-106.

Arndt, N.T., 1977. Ultrabasic magmas and high-degree melting of the mantle. Contributions to Mineralogy and Petrology 64 (2), 205-221.

Arndt, N.T., Lesher, C.M., Barnes, S.J., 2008. Komatiite. Cambridge, UK, Cambridge University Press.

Barnes, S.-J., Naldrett, A.J., Gorton, M.P., 1985. The origin of the fractionation of platinum-group elements in terrestrial magmas. Chemical Geology 53 (3-4), 303-323.

Barnes, S.J., Fiorentini, M.L., 2008. Iridium, ruthenium and rhodium in komatiites: Evidence for iridium alloy saturation. Chemical Geology 257 (1-2), 44-58.

Becker, H., Horan, M.F., Walker, R.J., Gao, S., Lorand, J.-P., Rudnick, R.L., 2006. Highly siderophile element composition of the Earth's primitive upper mantle: Constraints from new data on peridotite massifs and xenoliths. Geochimica et Cosmochimica Acta 70 (17), 4528-4550.

Begemann, F., Ludwig, K.R., Lugmair, G.W., Min., K., Nyquist, L.E., Patchett, P.J., Renne, P.R., Shih, C.-Y., Villa, I.M., Walker, R.J., 2001. Call for an improved set of decay constants for geochronological use. Geochimica et Cosmochimica Acta 65 (1), 111-121.

Bennett, V.C., Nutman, A.P., Esat, T.M., 2002. Constraints on mantle evolution from ^{187}Os/^{188}Os isotopic compositions of Archean ultramafic rocks from southern West Greenland (3.8 Ga) and Western Australia (3.46 Ga). Geochimica et Cosmochimica Acta 66 (14), 2615-2630.

Bezos, A., Lorand, J.-P., Humler, E., Gros, M., 2005. Platinum-group element systematics in Mid-Oceanic Ridge basaltic glasses from the Pacific, Atlantic, and Indian Oceans. Geochimica et Cosmochimica Acta 69 (10), 2613-2627.

Birck, J.L., Roy-Barman, M., Capman, F., 1997. Re-Os isotopic measurements at the femtomole level in natural samples. Geostandards Newsletter 20 (1), 19-27.

Borisov, A., Palme, H., 1997. Experimental determination of the solubility of platinum in silicate melts. Geochimica et Cosmochimica Acta 61 (20), 4349-4357.

Borisov, A., Palme, H., 2000. Solubilities of noble metals in Fe-containing silicate melts as derived from experiments in Fe-free systems. American Mineralogist 85 (11-12), 1665-1673.

Brandon, A.D., Creaser, R.A., Shirey, S.B., Carlson, R.W., 1996. Osmium recycling in subduction zones. Science 272 (5263), 861-864.

Brandon, A.D., Walker, R.J., Morgan, J.W., Norman, M.D., Prichard, H.M., 1998. Coupled ^{186}Os and ^{187}Os evidence for core-mantle interaction. Science 280 (5369), 1570-1573.

Brandon, A.D., Becker, H., Carlson, R.W., Shirey, S.B., 1999. Isotopic constraints on time scales and mechanisms of slab material transport in the mantle wedge: Evidence from the Simcoe mantle xenoliths, Washington, USA. Chemical Geology 160 (4), 387-407.

Brandon, A.D., Snow, J.E., Walker, R.J., Morgan, J.W., Mock, T.D., 2000. ^{190}Pt-^{186}Os and ^{187}Re-^{187}Os systematics of abyssal peridotites. Earth and Planetary Science Letters 177 (3-4), 319-335.

Brandon, A.D., Humayun, M., Puchtel, I.S., Zolensky, M., 2005a. Re-Os isotopic systematics and platinum group element composition of the Tagish Lake carbonaceous chondrite. Geochimica et Cosmochimica Acta 69 (6), 1619-1631.

Brandon, A.D., Walker, R.J., 2005. The debate over core-mantle interaction. Earth and Planetary Science Letters 232 (3-4), 211-225.

Brandon, A.D., Walker, R.J., Puchtel, I.S., Humayun, M., 2005b. Platinum-osmium isotope evolution of the Earth's mantle. Geochimica et Cosmochimica Acta 69, A392.

Brandon, A.D., Walker, R.J., Puchtel, I.S., 2006. Platinum-osmium isotope evolution of the Earth's mantle: Constraints from chondrites and Os-rich alloys. Geochimica et Cosmochimica Acta 70 (8), 2093-2103.

Brenan, J.M., McDonough, W.F., Dalpé, C., 2003. Experimental constraints on the partitioning of rhenium and some platinum-group elements between olivine and silicate melt. Earth and Planetary Science Letters 212 (1-2), 135-150.

Brenan, J.M., McDonough, W.F., Ash, R., 2005. An experimental study of the solubility and partitioning of iridium, osmium, and gold between olivine and silicate melt. Earth and Planetary Science Letters 237 (3-4), 855-872.

Brenan, J.M., 2008. Re-Os fractionation by sulfide melt-silicate melt partitioning: A new spin. Chemical Geology 248 (3-4), 140-165.

Brenan, J.M., Finnigan, C.F., McDonough, W.F., Homolova, V., 2012. Experimental constraints on the partitioning of Ru, Rh, Ir, Pt and Pd between chromite and silicate melt: The importance of ferric iron. Chemical Geology 302-303, 16-32.

Brügmann, G.E., Arndt, N.T., Hofmann, A.W., Tobschall, H.J., 1987. Noble metal abundances in komatiite suites from Alexo, Ontario, and Gorgona Island, Colombia. Geochimica et Cosmochimica Acta 51 (8), 2159-2169.

Campbell, I.H., Griffiths, R.W., Hill, R.I., 1989. Melting in an Archaean mantle plume: head it's basalts, tails it's komatiites. Nature 339 (6227), 697-699.

Chou, C.-L., Shaw, D.M., Crocket, J.H., 1983. Siderophile trace elements in the Earth's oceanic crust and upper mantle. Journal of Geophysical Research 88 (S2), A507-A518.

Cohen, A.S., Waters, F.G., 1996. Separation of osmium from geological materials by solvent extraction for analysis by thermal ionisation mass spectrometry. Analytica Chimica Acta 332 (2-3), 269-275.

Colodner, D.C., Boyle, E.A., Edmond, J.M., Thomson, J., 1992. Post-depositional mobility of platinum, iridium and rhenium in marine sediments. Nature 358 (6385), 402-404.

Connolly, B.D., Puchtel, I.S., Walker, R.J., Arevalo, R.J., Piccoli, P.M., Byerly, G.R., Robin-Popieul, C., Arndt, N.T., 2011. Highly Siderophile Element systematics of the 3.3 Ga Weltevreden komatiites, South Africa: implications for early Earth history. Earth and Planetary Science Letters 311 (3-4), 253-263.

Creaser, R.A., Papanastassiou, D.A., Wasserburg, G.J., 1991. Negative Thermal Ion Mass-Spectrometry of Osmium, Rhenium, and Iridium. Geochimica et Cosmochimica Acta 55 (1), 397-401.

Crocket, J.H., MacRae, W.E., 1986. Platinum-group element distribution in komatiitic and tholeiitic volcanic rocks from Munro Township, Ontario. Economic Geology 81 (5), 1242-1251.

Dann, J.C., 2000. The 3.5 Ga Komati Formation, Barberton Greenstone Belt, South Africa, Part I: New maps and magmatic architecture. South African Journal of Geology 103 (1), 47-68.

948 Fiorentini, M.L., Barnes, S.J., Maier, W.D., Burnham, O.M., Heggie, G., 2010. Global
949   Variability in the Platinum-group Element Contents of Komatiites. Journal of Petrology
950   52 (1), 83-112.
951 Fiorentini, M.L., Barnes, S.J., Maier, W.D., Burnham, O.M., Heggie, G., 2011. Global
952   Variability in the Platinum-group Element Contents of Komatiites. Journal of Petrology
953   52 (1), 83-112.
954 Fischer-Gödde, M., Becker, H., Wombacher, F., 2011. Rhodium, gold and other highly
955   siderophile elements in orogenic peridotites and peridotite xenoliths. Chemical Geology
956   280 (3-4), 365-383.
957 Fonseca, R.O.C., Mallmann, G., O'Neill, H.S.C., Campbell, I.H., 2007. How chalcophile is
958   rhenium? An experimental study of the solubility of Re in sulphide mattes. Earth and
959   Planetary Science Letters 260 (3-4), 537-548.
960 Fonseca, R.O.C., Mallmann, G., O'Neill, H.S.C., Campbell, I.H., Laurenz, V., 2011. Solubility of
961   Os and Ir in sulfide melt: Implications for Re/Os fractionation during mantle melting.
962   Earth and Planetary Science Letters 311 (3-4), 339-350.
963 Fonseca, R.O.C., Laurenz, V., Mallmann, G., Luguet, A., Hoehne, N., Jochum, K.P., 2012. New
964   constraints on the genesis and long-term stability of Os-rich alloys in the Earth's mantle.
965   Geochimica et Cosmochimica Acta 87, 227-242.
966 Foster, J.G., Lambert, D.D., Frick, L.R., Maas, R., 1996. Re-Os isotopic evidence for genesis of
967   Archaean nickel ores from uncontaminated komatiites. Nature 382 (6593), 703-706.
968 Frost, D.J., Liebske, C., Langenhorst, F., McCammon, C.A., Trönnes, R.G., Rubie, D.C., 2004.
969   Experimental evidence for the existence of iron-rich metal in the Earth's lower mantle.
970   Nature 428 (6981), 409-412.
971 Frost, D.J., Mann, U., Asahara, Y., Rubie, D.C., 2008. The redox state of the mantle during and
972   just after core formation. Philosophical Transactions of the Royal Society a-Mathematical
973   Physical and Engineering Sciences 366 (1883), 4315-4337.
974 Frost, D.J., McCammon, C.A., 2008. The redox state of Earth's mantle. In: (Ed.), Annual
975   Review of Earth and Planetary Sciences. Annual Reviews, Palo Alto, 36, 389-420.
976 Gangopadhyay, A., Walker, R.J., 2003. Re-Os systematics of the ca. 2.7 Ga komatiites from
977   Alexo, Ontario, Canada. Chemical Geology 196 (1-4), 147-162.
978 Gangopadhyay, A., Sproule, R.A., Walker, R.J., Lesher, C.M., 2005. Re-Os systematics of
979   komatiites and komatiitic basalts at Dundonald Beach, Ontario, Canada: Evidence for a
980   complex alteration history and implications of a late-Archean chondritic mantle source.
981   Geochimica et Cosmochimica Acta 69 (21), 5087-5098.
982 Gangopadhyay, A., Walker, R.J., Hanski, E., Solheid, P., 2006. Origin of Paleoproterozoic
983   Komatiites at Jeesiörova, Kittilä Greenstone Complex, Finnish Lapland. Journal of
984   Petrology 47 (4), 773-789.
985 Hamlyn, P.R., Keays, R.R., Cameron, W.E., Crawford, A.J., Waldron, H.M., 1985. Precious
986   metals in magnesian low-Ti lavas: Implications for metallogenesis and sulfur saturation
987   in primary magmas. Geochimica et Cosmochimica Acta 49 (8), 1797-1811.
988 Handler, M.R., Bennett, V.C., 1999. Behaviour of platinum-group elements in the subcontinental
989   mantle of eastern Australia during variable metasomatism and melt depletion.
990   Geochimica et Cosmochimica Acta 63 (21), 3597-3618.
991 Hanski, E., Walker, R.J., Huhma, H., Polyakov, G.V., Balykin, P.A., Hoa, T.T., Phuong, N.T.,
992   2004. Origin of the Permian-Triassic komatiites, northwestern Vietnam. Contributions to
993   Mineralogy and Petrology 147 (4), 453-469.

Hauri, E.H., Hart, S.R., 1993. Re-Os isotope systematics of HIMU and EMII oceanic island basalts from the south Pacific Ocean. Earth and Planetary Science Letters 114 (2-3), 353-371.

Horan, M.F., Walker, R.J., Morgan, J.W., Grossman, J.N., Rubin, A.E., 2003. Highly siderophile elements in chondrites. Chemical Geology 196 (1-4), 5-20.

Humayun, M., 2011. A model for osmium isotopic evolution of metallic solids at the core-mantle boundary. Geochemistry Geophysics Geosystems 12.

Huppert, H.E., Sparks, R.S.J., 1985. Cooling and contamination of mafic and ultramafic magmas during ascent through continental crust. Earth and Planetary Science Letterrs 74 (4), 371-386.

Kareem, K. (2005). Komatiites of the Weltevreden Formation, Barberton Greenstone Belt, South Africa: Implications for the chemistry and temperature of the Archean mantle. Department of Geology and Geophysics. Baton Rouge, Louisiana State University. **Doctor of Philosophy:** 233.

Keays, R.R., 1995. The role of komatiitic and picritic magmatism and S-saturation in the formation of ore deposits. Lithos 34 (1-3), 1-18.

Kimura, K., Lewis, R.S., Anders, S., 1974. Distribution of gold and rhenium between nickel-iron and silicate melts; implications for abundance of siderophile elements on the earth and moon. Geochimica et Cosmochimica Acta 38 (5), 683-701.

Lassiter, J.C., Hauri, E.H., 1998. Osmium-isotope variations in Hawaiian lavas: evidence for recycled oceanic lithosphere in the Hawaiian plume. Earth and Planetary Science Letters 164 (3-4), 483-496.

Liu, C.Z., Snow, J.E., Brugmann, G., Hellebrand, E., Hofmann, A.W., 2009. Non-chondritic HSE budget in Earth's upper mantle evidenced by abyssal peridotites from Gakkel ridge (Arctic Ocean). Earth and Planetary Science Letters 283 (1-4), 122-132.

Lorand, J.-P., Pattou, L., Gros, M., 1999. Fractionation of platinum-group elements and gold in the upper mantle: a detailed study in Pyrenean Orogenic lherzolites. Journal of Petrology 40 (6), 957-981.

Lorand, J.-P., Alard, O., 2001. Platinum-group element abundances in the upper mantle: new constraints from in situ and whole-rock analyses of Massif Central xenoliths (France). Geochimica et Cosmochimica Acta 65 (16), 2789-2806.

Lorand, J.P., Alard, O., Godard, M., 2009. Platinum-group element signature of the primitive mantle rejuvenated by melt-rock reactions: evidence from Sumail peridotites (Oman Ophiolite). Terra Nova 21 (1), 35-40.

Lowe, D.R., 1994. Accretionary history of the Archean Barberton Greenstone Belt (3.55-3.22 Ga), southern Africa. Geology 22 (12), 1099-1102.

Lowe, D.R., 1999. Geologic evolution of the Barberton Greenstone Belt and vicinity. In: Lowe, D.R. and Byerly, G.R. (Ed.), Geological Evolution of the Barberton Greenstone Belt. Geological Society of America, Special Paper 329, Boulder, 287-312.

Lowe, D.R., Byerly, G.R., 1999. Stratigraphy of the west-central part of the Barberton Greenstone Belt, South Africa. In: Lowe, D.R. and Byerly, G.R. (Ed.), Geological Evolution of the Barberton Greenstone Belt. Geological Society of America, Special Paper 329, Boulder, 1-36.

Lowe, D.R., Byerly, G.R., 2007. An overview of the geology of the Barberton Greenstone Belt and vicinity: Implications for early crustal development. In: Van Kranendonk, M.J.,

Smithies, R.H., and Bennett, V.C. (Ed.), Earth's Oldest Rocks. Elsevier, Amsterdam, 15, 481-526.

Ludwig, K.R. (2003). ISOPLOT 3.00. A geochronological toolkit for Microsoft Excel. Berkeley Geochronology Center Spec. Publ. **No. 4:** 70 pp.

Luguet, A., Lorand, J.-P., Seyler, M., 2003. Sulfide petrology and highly siderophile element geochemistry of abyssal peridotites: a coupled study of samples from the Kane Fracture Zone (45°W 23°20N, Mark Area, Atlantic Ocean). Geochimica et Cosmochimica Acta 67 (8), 1553-1570.

Luguet, A., Shirey, S.B., Lorand, J.-P., Horan, M.F., Carlson, R.W., 2007. Residual platinum-group minerals from highly depleted harzburgites of the Lherz massif (France) and their role in HSE fractionation of the mantle. Geochimica et Cosmochimica Acta 71 (12), 3082-3097.

Maier, W.D., Roelofse, F., Barnes, S.J., 2003. The concentration of the platinum-group elements in south African komatiites: Implications for mantle sources, melting regime and PGE fractionation during crystallization. Journal of Petrology 44 (10), 1787-1804.

Maier, W.D., Barnes, S.J., Campbell, I.H., Fiorentini, M.L., Peltonen, P., Barnes, S.J., Smithies, R.H., 2009. Progressive mixing of meteoritic veneer into the early Earth's deep mantle. Nature 460 (7255), 620-623.

Mavrogenes, J.A., O'Neill, H.S.C., 1999. The relative effects of pressure, temperature and oxygen fugacity on the solubility of sulfide in mafic magmas. Geochimica et Cosmochimica Acta 63 (7-8), 1173-1180.

McDonough, W.F., Sun, S.S., 1995. The composition of the Earth. Chemical Geology 120 (3-4), 223-253.

Meisel, T., Walker, R.J., Irving, A.J., Lorand, J.-P., 2001. Osmium isotopic compositions of mantle xenoliths: A global perspective. Geochimica et Cosmochimica Acta 65 (8), 1311-1323.

Meisel, T., Reisberg, L., Moser, J., Carignan, J., Melcher, F., Brügmann, G., 2003. Re-Os systematics of UB-N, a serpentinized peridotite reference material. Chemical Geology 201 (1-2), 161-179.

Meisel, T., Moser, J., 2004. Reference materials for geochemical PGE analysis: new analytical data for Ru, Rh, Pd, Os, Ir, Pt, and Re by isotope dilution ICP-MS in 11 geological reference materials. Chemical Geology 208 (1-4), 319-338.

Morgan, J.W., Wanderless, G.A., Petrie, R.K., Irving, A.J., 1981. Composition of the earth's upper mantle, I. Siderophile trace elements in ultramafic nodules. Tectonophysics 75 (1-2), 47-67.

Morgan, J.W., 1985. Osmium isotope constraints on Earth's late accretionary history. Nature 317 (6039), 703-705.

Morgan, J.W., 1986. Ultramafic xenoliths: Clues to Earth's late accretionary history. Journal of Geophysical Research 91 (B12), 12375-12387.

Peach, C.L., Mathez, E.A., Keays, R.R., 1990. Sulfide melt-silicate melt distribution coefficients for noble metals and other chalcophile elements as deduced from MORB; implications for partial melting. Geochimica et Cosmochimica Acta 54 (12), 3379-3389.

Pearson, D.G., Irvine, G.J., Ionov, D.A., Boyd, F.R., Dreibus, G.E., 2004. Re-Os isotope systematics and platinum-group-element fractionation during mantle melt extraction: A study of massif and xenolith peridotite suites. Chemical Geology 208, 29-59.

1084   Penniston-Dorland, S.C., Walker, R.J., Pitcher, L., Sorensen, S.S., 2012. Mantle-crust
1085   interactions in a paleosubduction zone: Evidence from highly siderophile element
1086   systematics of eclogite and related rocks. Earth and Planetary Science Letters 319, 295-
1087   306.
1088   Puchtel, I., Humayun, M., 2000. Platinum group elements in Kostomuksha komatiites and
1089   basalts: Implications for oceanic crust recycling and core-mantle interaction. Geochimica
1090   et Cosmochimica Acta 64 (24), 4227-4242.
1091   Puchtel, I.S., Haase, K.M., Hofmann, A.W., Chauvel, C., Kulikov, V.S., Garbe-Schönberg, C.D.,
1092   Nemchin, A.A., 1997. Petrology and geochemistry of crustally contaminated komatiitic
1093   basalts from the Vetreny Belt, southeastern Baltic Shield: Evidence for an early
1094   Proterozoic mantle plume beneath rifted Archean continental lithosphere. Geochimica et
1095   Cosmochimica Acta 61 (6), 1205-1222.
1096   Puchtel, I.S., Hofmann, A.W., Mezger, K., Jochum, K.P., Shchipansky, A.A., Samsonov, A.V.,
1097   1998. Oceanic plateau model for continental crustal growth in the Archaean: A case study
1098   from the Kostomuksha greenstone belt, NW Baltic Shield. Earth and Planetary Science
1099   Letters 155 (1-2), 57-74.
1100   Puchtel, I.S., Hofmann, A.W., Amelin, Y.V., Garbe-Schönberg, C.-D., Samsonov, A.V.,
1101   Shchipansky, A.A., 1999. Combined mantle plume - island arc model for the formation
1102   of the 2.9 Ga Sumozero-Kenozero greenstone belt, SE Baltic Shield: Isotope and trace
1103   element constraints. Geochimica et Cosmochimica Acta 63 (21), 3579-3595.
1104   Puchtel, I.S., Brügmann, G.E., Hofmann, A.W., 2001a. [187]Os-enriched domain in an Archaean
1105   mantle plume: Evidence from 2.8 Ga komatiites of the Kostomuksha greenstone belt,
1106   NW Baltic Shield. Earth and Planetary Science Letters 186 (3-4), 513-526.
1107   Puchtel, I.S., Brügmann, G.E., Hofmann, A.W., Kulikov, V.S., Kulikova, V.V., 2001b. Os
1108   isotope systematics of komatiitic basalts from the Vetreny belt, Baltic Shield: Evidence
1109   for a chondritic source of the 2.45 Ga plume. Contributions to Mineralogy and Petrology
1110   140 (5), 588-599.
1111   Puchtel, I.S., Humayun, M., 2001. Platinum group element fractionation in a komatiitic basalt
1112   lava lake. Geochimica et Cosmochimica Acta 17 (65), 2979-2993.
1113   Puchtel, I.S., Brandon, A.D., Humayun, M., 2004a. Precise Pt-Re-Os isotope systematics of the
1114   mantle from 2.7-Ga komatiites. Earth and Planetary Science Letters 224 (1-2), 157-174.
1115   Puchtel, I.S., Humayun, M., Campbell, A., Sproule, R., Lesher, C.M., 2004b. Platinum group
1116   element geochemistry of komatiites from the Alexo and Pyke Hill areas, Ontario,
1117   Canada. Geochimica et Cosmochimica Acta 68 (6), 1361-1383.
1118   Puchtel, I.S., Brandon, A.D., Humayun, M., Walker, R.J., 2005. Evidence for the early
1119   differentiation of the core from Pt-Re-Os isotope systematics of 2.8-Ga komatiites. Earth
1120   and Planetary Science Letters 237 (1-2), 118-134.
1121   Puchtel, I.S., Humayun, M., 2005. Highly siderophile element geochemistry of [187]Os-enriched
1122   2.8-Ga Kostomuksha komatiites, Baltic Shield. Geochimica et Cosmochimica Acta 69
1123   (6), 1607-1618.
1124   Puchtel, I.S., Humayun, M., Walker, R.J., 2007. Os-Pb-Nd isotope and highly siderophile and
1125   lithophile trace element systematics of komatiitic rocks from the Volotsk suite, SE Baltic
1126   Shield. Precambrian Research 158 (1-2), 119-137.
1127   Puchtel, I.S., Walker, R.J., Anhaeusser, C.R., Gruau, G., 2009a. Re-Os isotope systematics and
1128   HSE abundances of the 3.5 Ga Schapenburg komatiites, South Africa: Hydrous melting

1129   or prolonged survival of primordial heterogeneities in the mantle? Chemical Geology 262
1130   (3-4), 355-369.
1131 Puchtel, I.S., Walker, R.J., Brandon, A.D., Nisbet, E.G., 2009b. Pt-Re-Os and Sm-Nd isotope
1132   and HSE and REE systematics of the 2.7 Ga Belingwe and Abitibi komatiites.
1133   Geochimica et Cosmochimica Acta 73 (20), 6367-6389.
1134 Puchtel, I.S., Blichert-Toft, J., Touboul, M., Walker, R.J., Byerly, G., Nisbet, E.G., Anhaeusser,
1135   C.R., 2013. Insights into early Earth from Barberton komatiites: Evidence from lithophile
1136   isotope and trace element systematics. Geochimica et Cosmochimica Acta 108, 63-90.
1137 Rehkämper, M., Halliday, A.N., 1997. Development and application of new ion-exchange
1138   techniques for the separation of the platinum-group and other siderophile elements from
1139   geological samples. Talanta 44 (4), 663-672.
1140 Rehkämper, M., Halliday, A.N., Barfod, D., Fitton, J.G., 1997. Platinum-group element
1141   abundance patterns in different mantle environments. Science 278 (5343), 1595-1598.
1142 Rehkämper, M., Halliday, A.N., Alt, J., Fitton, J.G., Zipfel, J., Takazawa, E., 1999a. Non-
1143   chondritic platinum-group element ratios in oceanic mantle lithosphere: petrogenetic
1144   signature of melt percolation? Earth and Planetary Science Letters 172 (1-2), 65-81.
1145 Rehkämper, M., Halliday, A.N., Fitton, J.G., Lee, D.-C., Wieneke, M., Arndt, N.T., 1999b. Ir,
1146   Ru, Pt and Pd in basalts and komatiites: New constraints for the geochemical behavior of
1147   the platinum group elements in the mantle. Geochimica et Cosmochimica Acta 63 (22),
1148   3915-3934.
1149 Reisberg, L., Lorand, J.-P., 1995. Longevity of subcontinental mantle lithosphere from osmium
1150   isotope systematics in orogenic peridotite massifs. Nature 376 (6536), 159-162.
1151 Righter, K., 2003. Metal-silicate partitioning of siderophile elements and core formation in the
1152   early Earth. Annual Review of Earth and Planetary Sciences 31, 135-174.
1153 Shirey, S.B., Lewin, K.W., Berg, J.H., Carlson, R.W., 1994. Temporal changes in the sources of
1154   flood basalts: Isotopic and trace element evidence from the 1100 Ma old Keweenawan
1155   Mamainse Point Formation, Ontario, Canada. Geochimica et Cosmochimica Acta 58
1156   (20), 4475-4490.
1157 Shirey, S.B., 1997. Re-Os isotopic compositions of midcontinent rift system picrites:
1158   implications for plume-lithosphere interaction and enriched mantle sources. Canadian
1159   Journal of Earth Sciences 34 (4), 489-503.
1160 Shirey, S.B., Walker, R.J., 1998. The Re-Os isotope system in cosmochemistry and high-
1161   temperature geochemistry. Annual Reviews of Earth and Planetary Sciences 26, 423-500.
1162 Smoliar, M.I., Walker, R.J., Morgan, J.W., 1996. Re-Os ages of Group IIA, IIIA, IVA, and IVB
1163   iron meteorites. Science 271 (5762), 1099-1102.
1164 Snow, J.E., Reisberg, L., 1995. Os isotopic systematics of the MORB mantle: Results from
1165   altered abyssal peridotites. Earth and Planetary Science Letters 136 (3-4), 723-733.
1166 Stiegler, M.T., Cooper, M., Byerly, G.R., Lowe, D.R., 2012. Geochemistry and petrology of
1167   komatiites of the Pioneer Ultramafic Complex of the 3.3 Ga Weltevreden Formation,
1168   Barberton greenstone belt, South Africa. Precambrian Research 212, 1-12.
1169 Touboul, M., Puchtel, I.S., Walker, R.J., 2012. ^{182}W Evidence for Long-Term Preservation of
1170   Early Mantle Differentiation Products. Science 335, 1065-1069.
1171 Tsuru, A., Walker, R.J., Kontinen, A., Peltonen, P., Hanski, E., 2000. Re-Os isotopic systematics
1172   of the 1.95 Ga Jormua Ophiolite Complex, northeastern Finland. Chemical Geology 164
1173   (1-2), 123-141.

1174 Viljoen, M.J., Viljoen, R.P., 1969. The geology and geochemistry of the Lower Ultramafic Unit
1175   of the Onverwacht Group and a proposed new class of igneous rocks. Geological Society
1176   of South Africa Special Publication 2, 55-86.
1177 Viljoen, M.J., Viljoen, R.P., Smith, H.S., Erlank, A.J., 1983. Geological, textural and
1178   geochemical features of komatiitic flows from the Komati Formation. Geol. Soc. South
1179   Africa Spec. Publ. 9, 1-20.
1180 Wade, J., Wood, B.J., 2005. Core formation and the oxidation state of the Earth. Earth and
1181   Planetary Science Letters 236 (1-2), 78-95.
1182 Walker, R.J., Shirey, S.B., Stecher, O., 1988. Comparative Re-Os, Sm-Nd and Rb-Sr isotope and
1183   trace element systematics for Archean komatiite flows from Munro Township, Abitibi
1184   belt, Ontario. Earth and Planetary Science Letters 87 (1-2), 1-12.
1185 Walker, R.J., Carlson, R.W., Shirey, S.B., Boyd, F.R., 1989. Os, Sr, Nd, and Pb isotope
1186   systematics of southern African peridotite xenoliths: Implications for the chemical
1187   evolution of subcontinental mantle. Geochimica et Cosmochimica Acta 53 (7), 1583-
1188   1595.
1189 Walker, R.J., Echeverria, L.M., Shirey, S.B., Horan, M.F., 1991. Re-Os isotopic constraints on
1190   the origin of volcanic rocks, Gorgona Island, Colombia: Os-isotopic evidence for ancient
1191   heterogeneities in the mantle. Contributions to Mineralogy and Petrology 107 (2), 150-
1192   162.
1193 Walker, R.J., Morgan, J.W., Horan, M.F., 1995. ^{187}Os enrichment in some plumes: evidence for
1194   core-mantle interaction? Science 269 (5225), 819-822.
1195 Walker, R.J., Hanski, E., Vuollo, J., Liipo, J., 1996. The Os isotopic composition of Proterozoic
1196   upper mantle: evidence for chondritic upper mantle from the Outokumpu ophiolite,
1197   Finland. Earth and Planetary Science Letters 141 (1-4), 161-173.
1198 Walker, R.J., Morgan, J.W., Beary, E.S., Smoliar, M.I., Czamanske, G.K., Horan, M.F., 1997.
1199   Applications of the ^{190}Pt-^{186}Os isotope system to geochemistry and cosmochemistry.
1200   Geochimica et Cosmochimica Acta 61 (22), 4799-4807.
1201 Walker, R.J., Storey, M., Kerr, A.C., Tarney, J., Arndt, N.T., 1999. Implications of ^{187}Os isotopic
1202   heterogeneities in a mantle plume: Evidence from Gorgona Island and Curaçao.
1203   Geochimica et Cosmochimica Acta 63 (5), 713-728.
1204 Walker, R.J., Stone, W.E., 2001. Os isotope constraints on the origin of the 2.7 Ga Boston Creek
1205   Flow, Ontario, Canada. Chemical Geology 175 (3-4), 567-579.
1206 Walker, R.J., Prichard, H.M., Ishivatari, A., Pimentel, M., 2002. The osmium isotopic
1207   composition of the convecting upper mantle deduced from ophiolite chromites.
1208   Geochimica et Cosmochimica Acta 66 (2), 329-345.
1209 Walker, R.J., Brandon, A.D., Bird, J.M., Piccoli, P.M., McDonough, W.F., Ash, R.D., 2005.
1210 ^{187}Os-^{186}Os systematics of Os-Ir-Ru alloy grains from southwestern Oregon. Earth and
1211   Planetary Science Letterrs 230 (1-2), 211-226.
1212 Walker, R.J., 2009. Highly siderophile elements in the Earth, Moon and Mars: Update and
1213   implications for planetary accretion and differentiation. Chemie der Erde - Geochemistry
1214   69 (2), 101-125.
1215 Wilson, A.H., Shirey, S.B., Carlson, R.W., 2003. Archaean ultra-depleted komatiites formed by
1216   hydrous melting of cratonic mantle. Nature 423 (6942), 858-860.
1217 Woodland, S.J., Pearson, D.G., Thirlwall, M.F., 2002. A platinum-group element and Re-Os
1218   isotope investigation of siderophile element recycling in subduction zones: Comparison

1219   of Grenada, Lesser Antilles Arc, and the Izu-Bonin Arc. Journal of Petrology 43 (1), 171-
1220   198.
1221

Figure 1. Re-Os isochron diagrams for the Komati (upper panel) and Weltevreden Fm. (lower panel) komatiites. The data set for the latter include both our data and those reported by Connolly et al. (2011), as discussed in the text. Two cumulate samples (BV14 from Komati and SA501-7 from Weltevreden) plot well below the respective regression lines and were excluded from the regression calculations for reasons discussed in the text. The uncertainties on the ages and the initial isotopic ratios ($2\sigma_{mean}$) are derived from the ISOPLOT regression calculations.

Figure 2. Pt-Os isotopic data for the Komati (upper panel) and Weltevreden (lower panel) komatiite systems. The initial $^{186}Os/^{188}Os$ ratios represent averages of the initial $^{186}Os/^{188}Os$ ratios for each individual sample analyzed calculated using measured $^{186}Os/^{188}Os$ and $^{190}Pt/^{188}Os$. The uncertainties on the average initial $^{186}Os/^{188}Os$ ratios for each system are determined by the external long-term reproducibility for the in-house Johnson-Matthey Os standard (±14 ppm) divided by square root of the number of samples analyzed for each system. The chondritic reference lines for the respective emplacement ages of 3484 Ma and 3263 Ma are constructed on the basis of parameters from Brandon et al. (2006), as discussed in the text.

Figure 3. Variations of HSE abundances as a function of MgO contents in the Komati and Weltevreden whole-rock komatiite samples and pure olivine separates. The regression lines were fitted through the whole-rock and olivine separate data using ISOPLOT. The samples that plot off the regression lines were not included into the regression calculations.

Figure 4. Normalized to an average CI chondrite Orgueil (Horan et al., 2003) HSE abundances in whole-rock komatiite samples from the Komati (upper left panel) and Weltevreden (lower left panel) Fms., as well as in the calculated emplaced komatiite lavas from both localities (upper right panel).

Figure 5. Normalized to an average CI chondrite Orgueil (Horan et al., 2003) HSE abundances in olivine (upper panel) and chromite (lower panel) separates from the Komati and Weltevreden komatiites.

Figure 6a. Initial $^{187}Os/^{188}Os$ isotopic compositions, expressed in $\gamma^{187}Os$ terms, of best studied Archean komatiite systems, and of olivine and chromite separates from Isua peridotites, plotted as a function of age. The $^{187}Os/^{188}Os$ isotopic data for the komatiite systems are from Foster et al. (1996), Puchtel et al. (2001a; 2001b), Puchtel et al. (2004a), Puchtel et al. (2005), Puchtel et al. (2007), Puchtel et al. (2009a; 2009b) and this study, and for the Isua peridotites – from Bennett et al. (2002). These data are compared with those for the average PM estimate from Meisel et al. (2001), and with the data for an average abyssal peridotite from Snow and Reisberg (1995), Brandon et al. (2000), and Liu et al. (2009). **b.** Initial $^{186}Os/^{188}Os$ isotopic compositions, expressed in $\varepsilon^{186}Os$ terms, of Archean komatiite systems studied to-date, plotted as a function of age. The $^{186}Os/^{188}Os$ isotopic data for the komatiite

1266   systems are from Puchtel et al. (2004a), Puchtel et al. (2005), Puchtel et al. (2009b) and this
1267   study. The parameters for the model PM reservoir were adopted from Brandon et al. (2006)
1268   and for the model DMM reservoir – from Brandon et al. (2000). The uncertainties on the Os
1269   initial isotopic ratios are $2\sigma_{mean}$.
1270

1271   **Figure 7.** Normalized to an average CI chondrite Orgueil (Horan et al., 2003) HSE abundances
1272   in the sources of the Komati and Weltevreden komatiite systems calculated using the
1273   projection technique of Puchtel et al. (2004b) and Puchtel and Humayun (2005) described in
1274   the text, and in an average Komati-Weltevreden komatiite source. The Pt abundances are
1275   corrected for Pt-Fe alloy fractionation, as discussed in the text. The average late Archean
1276   komatiite source from Puchtel et al. (2009b) and a PM estimate of Becker et al. (2006) are
1277   plotted for comparison. The uncertainties are $2\sigma_{mean}$.
1278

1279   **Figure 8.** Calculated total Pt and Pd abundances in the sources of the Komati and Weltevreden
1280   komatiite systems from this study plotted as a per cent of the total Pt and Pd abundances in
1281   the estimates of the modern PM of Becker et al. (2006). In the calculations of the totals, the
1282   relative weight of Pd contribution to the total was normalized to Pt on the basis of its relative
1283   abundance in an average CI chondrite Orgueil (Horan et al., 2003). The total Pt and Pd
1284   abundances present in the sources of the best-studied late Archean komatiite systems
1285   compiled from the data of Puchtel and Humayun (2001, 2005), Puchtel et al. (2004a; 2004b),
1286   Puchtel et al. (2005), Puchtel et al. (2007), and Puchtel et al. (2009b) and for the 3.55 Ga
1287   Schapenburg komatiite system from Puchtel et al. (2009a) are plotted for comparison. The
1288   uncertainties are $2\sigma_{mean}$.
1289
1290

1291 *Table 1.* HSE abundances (ppb) and $^{187}Os/^{188}Os$ ratios in the UB-N and GP-13 reference
1292 materials.
1293

Lab	*n*	Re	Os	Ir	Ru	Pt	Pd	$^{187}Os/^{188}Os$
UB-N								
IGL [1]	5	0.211±0.010	3.79±0.27	3.55±0.32	6.88±0.37	7.71±0.07	6.10±0.10	0.12706±16
IGL [2]	4	0.205±0.004	3.51±0.12	3.26±0.13	6.51±0.33	7.00±0.23	5.85±0.26	0.12737±25
Chicago [3]	6	0.199±0.023	3.72±0.35	3.62±0.22	7.42±0.52	7.52±0.27	6.11±0.23	
Leoben [4]	14	0.210±0.004	3.85±0.13	3.38±0.22	6.30±0.30	7.42±0.30	6.11±0.18	
GP-13								
IGL [1]	6	0.307±0.010	3.77±0.11	3.52±0.25	6.89±0.09	7.54±0.34	5.92±0.16	0.12644±9
Chicago [3]	3	0.283±0.003	3.70±0.02	3.42±0.08	7.03±0.38	6.82±0.48	5.34±0.10	
Leoben [4]	7	0.312±0.023	4.06±0.07	3.40±0.18	6.05±0.95	6.38±1.09	5.80±0.36	
Durham [5]	8	0.330±0.007	3.87±0.24	3.56±0.46	6.97±0.33	7.00±0.74	5.64±0.50	0.12637±42

1294 [1] This study, CT digestion, ID-ICP-MS (Re and PGE) and ID-TIMS (Os) techniques.
1295 [2] Becker et al. (2006), CT digestion at 345°C in pressurized vessels, ID-ICP-MS (Re and PGE)
1296 and ID-TIMS (Os) techniques.
1297 [3] Puchtel et al. (2005), CT digestion, ID-ICP-MS techniques.
1298 [4] Meisel et al. (2003) and Meisel and Moser (2004), high pressure asher (HPA) digestion ID-
1299 ICP-MS (Re and PGE) and ID-TIMS (Os) techniques.
1300 [5] Pearson et al. (2004), CT and HPA digestion ID-ICP-MS technique.
1301 *n* – number of analyses. Errors quoted at $2\sigma_{mean}$
1302
1303
1304

1305 ***Table 2.*** Re-Os isotopic data for the Komati and Weltevreden Fm. whole-rock komatiite
1306 samples and olivine and chromite separates.
1307

Sample	Re (ppb)	Os (ppb)	$^{187}Re/^{188}Os$	$\pm 2\sigma$	$^{187}Os/^{188}Os$	$\pm 2\sigma$	$\gamma^{187}Os(T)$
Komati Fm.							
BV02	0.0768	1.307	0.2830	0.0028	0.12028	0.00006	+0.36
BV05	0.0501	1.188	0.2030	0.0029	0.11540	0.00007	+0.26
BV08	0.0708	1.242	0.2745	0.0027	0.11964	0.00006	+0.23
BV09	0.1229	1.098	0.5400	0.0054	0.13579	0.00006	+0.51
BV01	0.1157	2.153	0.2585	0.0026	0.11872	0.00006	+0.26
BV03	0.0354	0.9443	0.1802	0.0018	0.11430	0.00005	+0.52
BV10	0.0410	1.263	0.1560	0.0016	0.11296	0.00006	+0.62
BV13	0.0217	1.827	0.0570	0.0066	0.10670	0.00006	+0.28
BV14	0.2745	1.6097	0.8216	0.0082	0.14461	0.00006	-7.3
BV15_A	0.0525	3.109	0.0812	0.0008	0.10793	0.00006	+0.08
BV15_B	0.0461	3.422	0.0648	0.0006	0.10745	0.00006	+0.56
BV15_IC_A*			0.0754	0.0008	0.10800	0.00006	+0.48
BV15_IC_A**					0.108038	0.000003	
BV15_IC_B*			0.0832	0.0008	0.10828	0.00006	+0.30
BV15_IC_B**					0.108284	0.000001	
BV16_A	0.1790	2.425	0.3555	0.0036	0.12450	0.00008	+0.25
BV16_B	0.1901	2.442	0.3756	0.0038	0.12584	0.00008	+0.39
BV16_IC*			0.3779	0.0038	0.12582	0.00008	+0.23
BV16_IC**					0.125851	0.000001	
BV03 Ol	0.0145	0.6612	0.1055	0.0030	0.10948	0.00007	+0.17
BV10 Ol	0.0033	0.3557	0.0452	0.0052	0.10569	0.00005	-0.01
BV03 Chr	0.2414	17.87	0.0649	0.0066	0.10714	0.00011	+0.26
BV10 Chr	0.2376	51.33	0.0222	0.0025	0.10484	0.00008	+0.50

1308
1309

1310 **Table 2.** *(Continued)*

1311

Sample	Re (ppb)	Os (ppb)	^{187}Re/^{188}Os	±2σ	^{187}Os/^{188}Os	±2σ	γ^{187}Os(T)
Weltevreden Fm.							
564-6	*0.317*	*1.238*	*1.242*	*0.012*	*0.17388*	*0.00009*	*-0.05*
501-3	*0.309*	*1.384*	*1.080*	*0.011*	*0.16486*	*0.00009*	*-0.03*
564-4	*0.331*	*0.9713*	*1.655*	*0.017*	*0.19693*	*0.00010*	*-0.09*
564-5	*0.284*	*1.457*	*0.9435*	*0.0094*	*0.15710*	*0.00009*	*-0.16*
12--2	*0.339*	*1.214*	*1.355*	*0.014*	*0.18025*	*0.00013*	*+0.01*
501-1_A	*0.153*	*10.77*	*0.0682*	*0.0007*	*0.10816*	*0.00005*	*-0.21*
501-1_B	0.143	10.11	0.0680	0.0007	0.10832	0.00006	-0.04
501-1_IC_A*			0.0660	0.0007	0.10808	0.00007	-0.16
501-1_IC_A**					0.107955	0.000002	
501-1_IC_B*			0.0670	0.0007	0.10809	0.00006	-0.21
501-1_IC_B**					0.108106	0.000001	
501-7	*0.258*	*1.074*	*1.158*	*0.006*	*0.14811*	*0.00007*	*-20.2*
501-8	0.183	0.9819	0.9023	0.0090	0.15474	0.00010	-0.22
501-9	*0.171*	*1.015*	*0.8122*	*0.0081*	*0.14979*	*0.00007*	*-0.15*
501-10	*0.162*	*6.621*	*0.1174*	*0.0012*	*0.11096*	*0.00005*	*-0.15*
501-10_IC*			0.1036	0.0010	0.11030	0.00005	-0.05
501-10_IC**					0.110303	0.000001	
427-5	0.159	7.354	0.1038	0.0010	0.11017	0.00005	-0.18
564-2	*0.141*	*2.660*	*0.2556*	*0.0026*	*0.11857*	*0.00006*	*-0.26*
564-3	*0.0664*	*3.066*	*0.1042*	*0.0010*	*0.11024*	*0.00005*	*-0.14*
12--6	*0.162*	*4.345*	*0.1794*	*0.0018*	*0.11452*	*0.00007*	*-0.06*
12--7	0.175	5.089	0.1656	0.0017	0.11360	0.00007	-0.20
12--8	*0.122*	*4.699*	*0.1246*	*0.0012*	*0.11139*	*0.00005*	*-0.12*
12--8_IC*			0.1254	0.0013	0.11146	0.00006	-0.10
12--8_IC**					0.111500	0.000001	
501-1 Ol	*0.0184*	*8.552*	*0.0103*	*0.0003*	*0.10501*	*0.00005*	*-0.13*
501-8 Ol	0.0033	2.385	0.0067	0.0010	0.10483	0.00007	-0.10
12-6 Ol	0.0029	3.321	0.0042	0.0007	0.10467	0.00007	-0.13

1312 *Note.* The initial γ^{187}Os were calculated for the ages *T* defined by the isochrons for the Komati
1313 (3484 Ma) and Weltevreden (3263 Ma) komatiite systems using the model parameters specified
1314 in the text. Italicized values represent data from Connolly et al. (2011) reported here for
1315 convenience.
1316 (*) Averages for the spiked aliquots of the unspiked digestions processed for the Pt-Os study (see
1317 **Table 3**) to determine the Re/Os and Pt/Os ratios.
1318 (**) Data from the high-precision runs for the Pt-Os study (see **Table 3**). These data are shown
1319 here for comparison with the data for the spiked runs only and were not used for the isochron
1320 calculations.

1321

49

1322 *Table 3.* High-precision osmium isotopic data and Re/Os and Pt/Os ratios for the Komati and
1323 Weltevreden komatiite systems.
1324

Sample	$^{187}Re/^{188}Os$	$^{190}Pt/^{188}Os$	$^{184}Os/^{188}Os$	$^{186}Os/^{188}Os$	$^{187}Os/^{188}Os$	$\varepsilon^{186}Os(T)$	$\gamma^{187}Os(T)$
Komati Fm.							
BV15_A	0.0754	0.001021	0.001316±4	0.1198336±25	0.1080382±29	-0.12±0.21	+0.52
BV15_B	0.0832	0.001172	0.001310±1	0.1198344±9	0.1082836±13	-0.11±0.07	+0.30
BV16	0.378	0.001205	0.001307±1	0.1198343±7	0.1258510±09	-0.13±0.06	+0.26
Weltevreden Fm.							
501-1_A	0.0660	0.000337	0.001306±7	0.1198344±11	0.1079550±24	+0.21±0.10	-0.28
501-1_B	0.0670	0.000334	0.001312±5	0.1198346±21	0.1081057±13	+0.22±0.18	-0.19
501-10	0.104	0.000556	0.001305±2	0.1198354±18	0.1103029±09	+0.20±0.15	-0.05
12-8	0.125	0.000800	0.001302±3	0.1198373±9	0.1114998±13	+0.26±0.08	-0.06

1325

1326   **Note.** The uncertainties on the Re/Os and Pt/Os ratios are 1.0% relative. The initial $\varepsilon^{186}Os$
1327 and $\gamma^{187}Os$ values were calculated for the emplacement ages of 3484 Ma (Komati Fm.) or 3263
1328 Ma (Weltevreden Fm.) defined by the respective Re-Os isochrons.
1329
1330
1331
1332

1333 *Table 4.* Highly siderophile element abundance data (ppb) for the Komati and Weltevreden Fm.
1334 whole-rock komatiite samples and mineral separates.
1335

Sample	Re	Os	Ir	Ru	Pt	Pd	$(Os/Ir)_N$	$(Pd/Ir)_N$
Komati system. *Chilled margin*								
BV02	0.0818	1.391	1.34	3.53	5.00	4.62	**1.01**	**2.70**
Olivine spinifex								
BV05	0.0532	1.262	1.40	3.72	5.29	4.98	**0.88**	**2.79**
BV08	0.0754	1.322	1.42	3.71	4.84	4.77	**0.90**	**2.63**
BV09	0.129	1.148	1.31	3.51	5.93	5.77	**0.85**	**3.45**
Olivine cumulates								
BV01	0.124	2.315	2.03	3.68	4.06	3.99	**1.11**	**1.54**
BV03	0.0374	0.9990	0.979	3.13	3.26	3.49	**0.99**	**2.78**
BV10	0.0438	1.352	1.20	3.56	3.33	3.55	**1.09**	**2.31**
BV13	0.0233	1.965	1.78	4.90	3.21	3.21	**1.07**	**1.41**
BV14	0.296	1.736	1.69	6.75	4.01	4.20	**1.00**	**1.94**
BV15	0.0563	3.333	2.95	4.36	3.40	3.51	**1.10**	**0.93**
Replicate	0.0495	3.669	3.09	4.33	3.40	3.49	**1.15**	**0.88**
BV16	0.192	2.603	2.46	4.36	3.84	3.79	**1.03**	**1.21**
Replicate	0.204	2.622	2.50	4.65	3.81	3.94	**1.02**	**1.23**
Olivine and chromite separates								
BV03 Ol	0.0145	0.6612	0.608	2.72	0.268	0.400	**1.05**	**0.51**
BV10 Ol	0.0034	0.3557	0.363	2.69	0.0800	0.0813	**0.95**	**0.17**
BV03 Chr	0.241	17.87	20.5	236	6.21	4.10	**0.84**	**0.16**
BV10 Chr	0.238	51.33	51.9	400	6.69	1.22	**0.96**	**0.018**

1336
1337

1338 *Table 4. (Continued).*
1339

Sample	Re	Os	Ir	Ru	Pt	Pd	$(Os/Ir)_N$	$(Pd/Ir)_N$
Weltevreden system. *Chilled margin*								
564-6	*0.345*	*1.35*	*1.40*	*6.55*	*9.10*	*7.04*	*0.90*	*3.37*
Olivine spinifex								
501-3	*0.333*	*1.49*	*1.56*	*5.94*	*8.58*	*6.60*	*0.90*	*2.85*
564-4	*0.357*	*1.05*	*1.13*	*6.25*	*9.52*	*7.46*	*0.87*	*4.45*
564-5	*0.308*	*1.58*	*1.57*	*6.14*	*8.43*	*6.65*	*0.94*	*2.84*
12-2	*0.366*	*1.31*	*1.40*	*6.54*	*9.60*	*7.56*	*0.88*	*3.62*
Olivine cumulate								
501-1	*0.170*	*11.9*	*10.6*	*6.32*	*4.35*	*3.33*	*1.05*	*0.21*
Replicate	0.159	11.3	9.23	6.67	4.45	3.15	**1.14**	**0.23**
501-7	*0.284*	*1.18*	*1.10*	*5.48*	*4.98*	*3.98*	*1.01*	*2.42*
501-8	0.201	1.08	1.12	6.07	4.90	3.52	**0.90**	**2.11**
501-9	*0.187*	*1.11*	*1.05*	*5.29*	*4.74*	*3.67*	*1.00*	*2.35*
501-10	*0.173*	*7.07*	*6.00*	*5.49*	*4.53*	*3.53*	*1.11*	*0.40*
427-5	0.175	8.10	6.51	5.68	4.64	3.31	**1.17**	**0.34**
564-2	*0.154*	*2.89*	*2.92*	*9.06*	*4.37*	*3.34*	*0.93*	*0.77*
564-3	*0.0720*	*3.32*	*3.42*	*8.98*	*4.55*	*3.32*	*0.91*	*0.65*
12-6	*0.177*	*4.75*	*4.35*	*6.12*	*4.75*	*3.78*	*1.02*	*0.58*
12-7	0.194	5.65	4.83	6.12	4.69	3.33	**1.10**	**0.46**
12-8	*0.134*	*5.18*	*4.84*	*6.66*	*4.29*	*3.23*	*1.01*	*0.45*
Olivine separates								
501-1 Ol	0.0184	8.55	7.42	5.92	0.701	0.457	**1.08**	**0.041**
501-8 Ol	0.0033	2.39	2.18	7.11	0.129	0.0789	**1.03**	**0.024**
12-6 Ol	0.0029	3.32	2.92	6.51	0.441	0.0794	**1.07**	**0.018**

1340
1341 *Note.* Abundances are re-calculated on an anhydrous basis. Italicized values represent data from
1342 Connolly et al. (2011) reported here for convenience. The Os/Ir and Pd/Ir ratios are normalized
1343 relative to average Orgueil values from Horan et al. (2003).
1344
1345

1346   *Table 5.* Calculated HSE abundances (ppb) in the emplaced lavas and mantle sources of the
1347   Komati and Weltevreden komatiite systems.
1348

	Re	**Os**	**Ir**	**Ru**	**Pt**	**Pd**	**(Os/Ir)$_N$**	**(Pd/Ir)$_N$**
Komati system								
Emplaced lava		1.3±0.1	1.4±0.1	3.6±0.2	4.8±0.4	4.7±0.4	0.93±0.05	2.7±0.2
Source	0.29±0.10	3.3±1.1	3.5±1.2	3.5±0.3	2.9±0.2	2.9±0.2	0.93±0.33	0.83±0.29
Source Pt-corrected	0.29±0.10	3.3±1.1	3.5±1.2	3.5±0.3	5.9±0.9	2.9±0.2	0.93±0.33	0.83±0.29
Weltevreden system								
Emplaced lava	0.33±0.03	1.4±0.1	1.5±0.1	6.3±0.2	8.5±0.5	6.6±0.5	0.94±0.08	3.5±0.2
Source	0.23±0.02	2.7±0.2	2.9±0.3	6.0±0.3	6.0±0.4	4.6±0.3	0.94±0.08	1.6±0.1
Source Pt-corrected	0.23±0.02	2.7±0.2	2.9±0.3	6.0±0.3	4.9±0.7	4.6±0.3	0.94±0.08	1.6±0.1

1349
1350   *Note.* Re abundances in the emplaced Komati lava could not be calculated due to Re post-
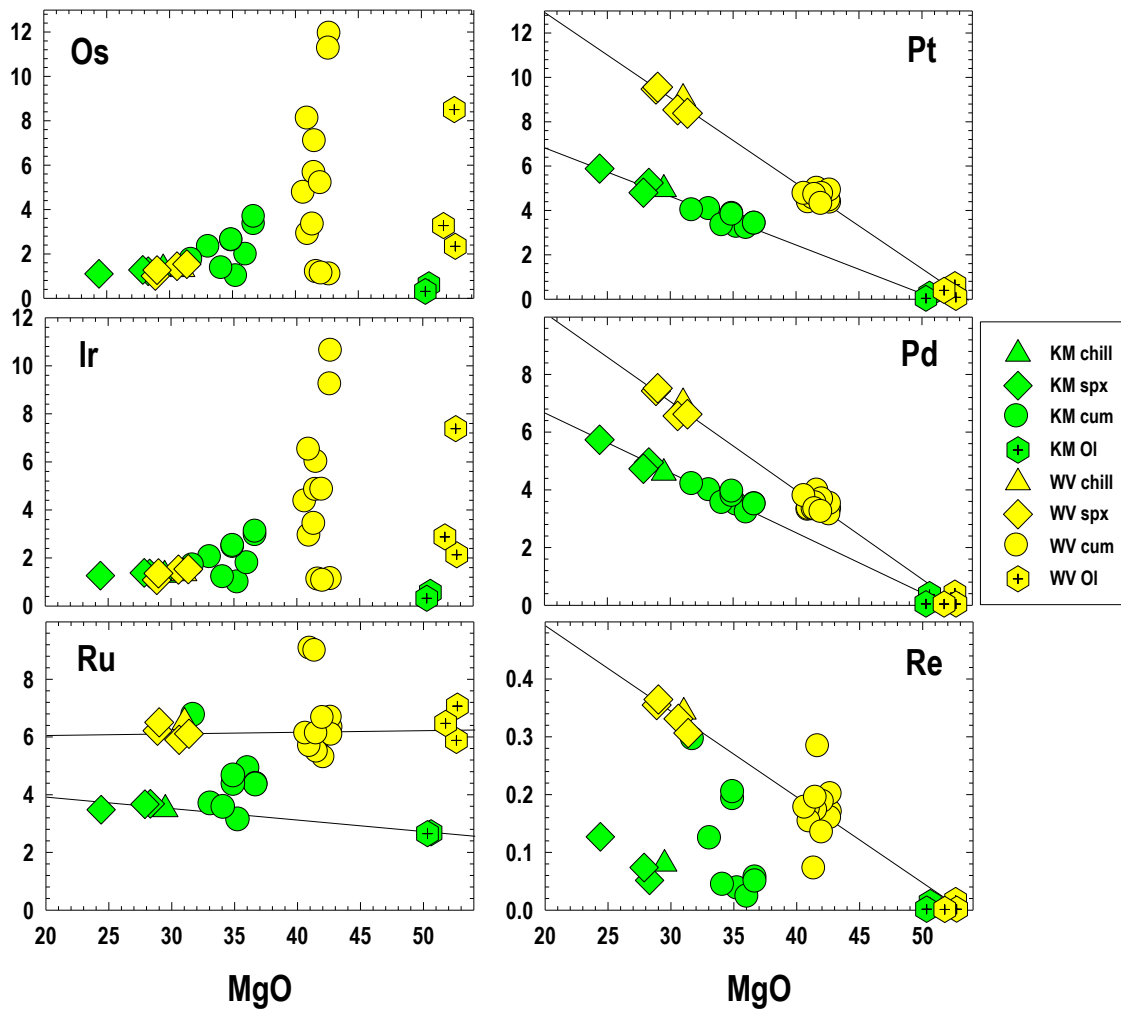1351   emplacement mobility.
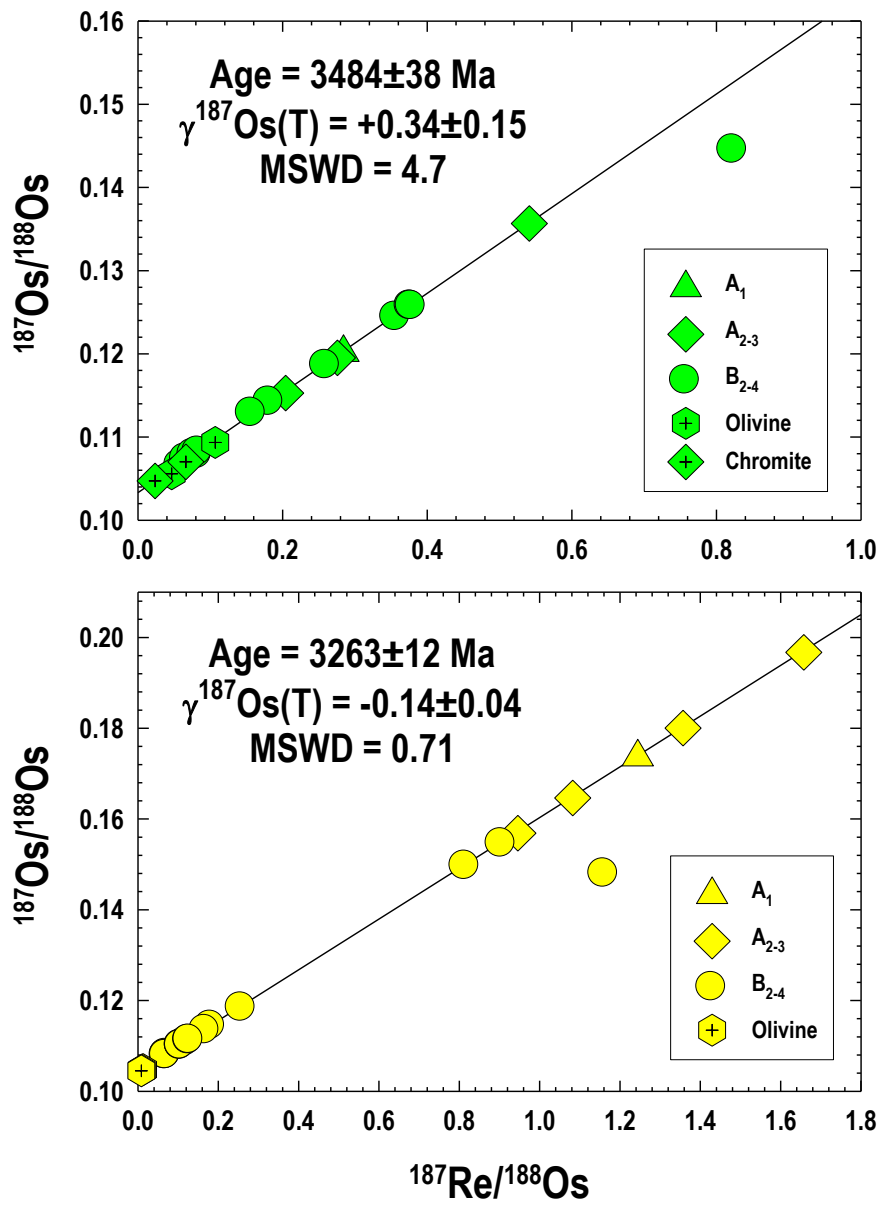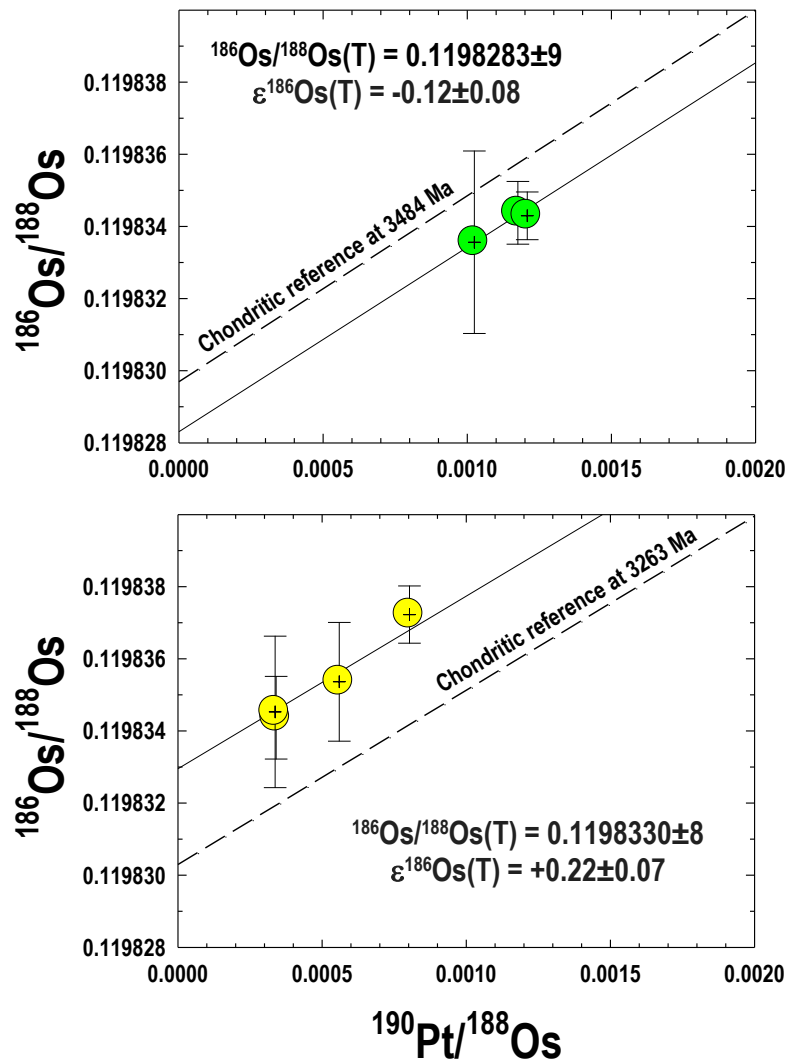
Figure(s)

Figure 1.

Figure 2.

Figure 3.
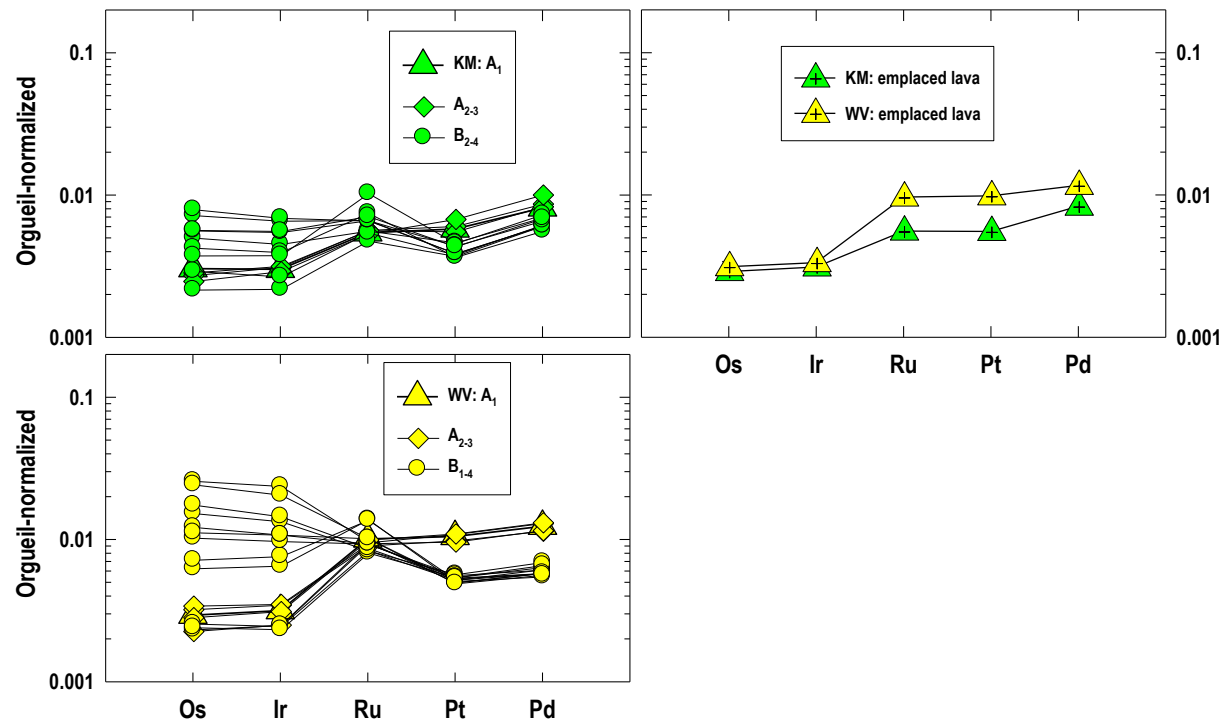
Figure 4.
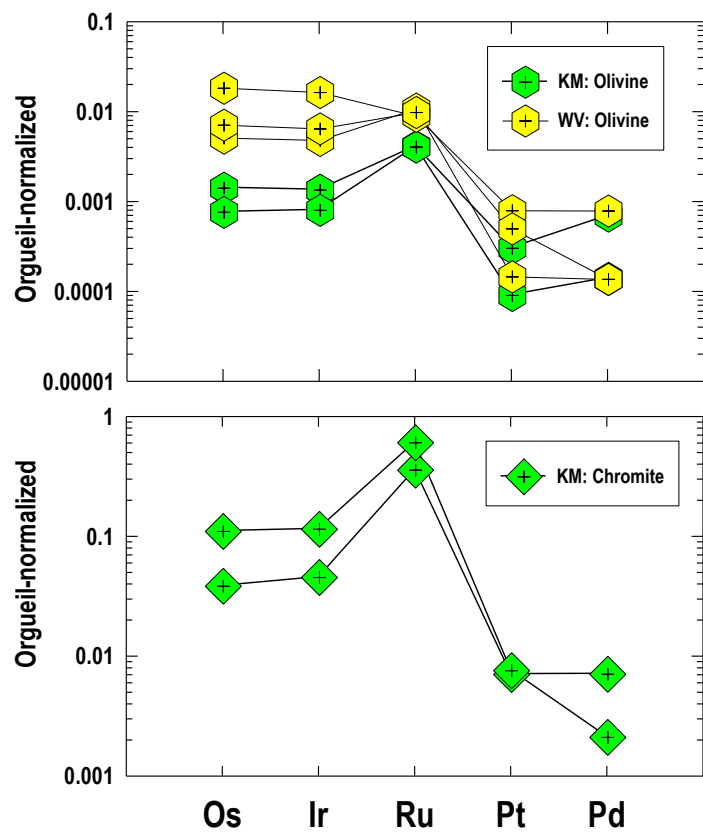
Figure 5.
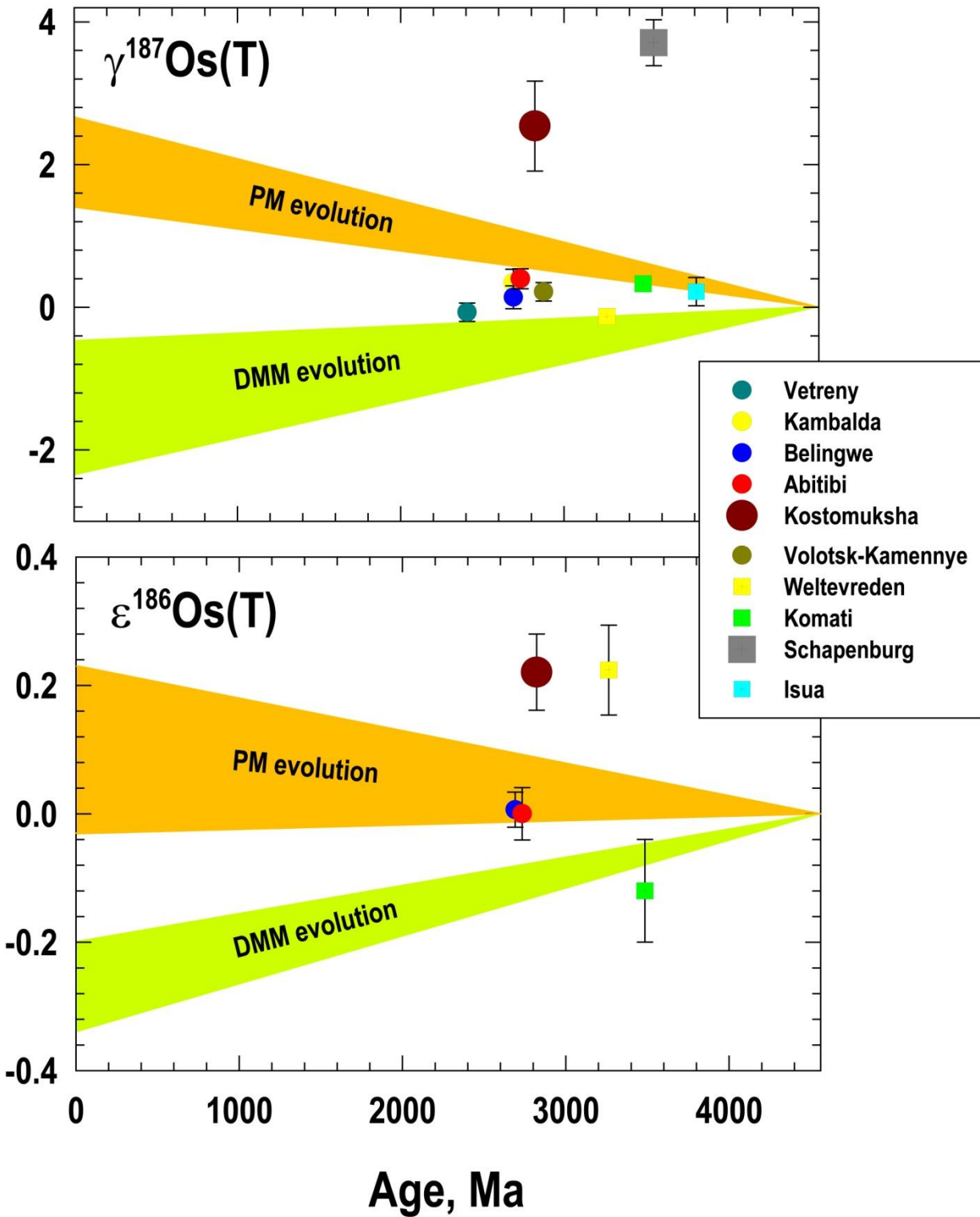
Figure 6.

Figure 7.

Figure 8.